AIMS Mathematics, 11(1): 1489–1526.
DOI:10.3934/math.2026063
Received: 13 November 2025
Revised: 21 December 2025
Accepted: 07 January 2026
Published: 19 January 2026

https://www.aimspress.com/journal/Math

Research article

Modeling within-host dynamics of two competing viruses with distinct target-cell populations

N. H. AlShamrani[1,*] **and A. M. Elaiw**[2]

[1] Department of Mathematics and Statistics, College of Science, University of Jeddah, P.O. Box 80327, Jeddah 21589, Saudi Arabia

[2] Department of Mathematics, Faculty of Science, King Abdulaziz University, P.O. Box 80203, Jeddah 21589, Saudi Arabia

* **Correspondence:** Email: nhalshamrani@uj.edu.sa.

Abstract: Since some viruses share transmission routes, coinfection can occur. While most models assume one target cell, many viruses infect and replicate in multiple cell types. The purpose of this study is to develop and analyze a model describing coinfection by two viruses that grow and compete within two distinct target-cell populations. We prove that the proposed model is mathematically well-defined and admits unique, biologically meaningful solutions. Using the next-generation matrix method, we derive expressions for the basic reproduction numbers corresponding to virus type 1 single infection (R_1), virus type 2 single infection (R_2), and two-virus coinfection (R_0). The model usually admits an infection-free equilibrium. The existence conditions for the virus type 1 single-infection, virus type 2 single-infection, and two-virus coexistence equilibria are also established. Applying the Lyapunov direct method, we demonstrate the global stability of all steady states. The obtained results reveal new insights into the factors that allow two viruses to coexist in a stable state, thereby enabling the possibility of chronic coinfections. The model is further extended to examine the influence of two reverse transcriptase (RT) inhibitors and to explore the role of a second target-cell population in two-virus codynamics. We find that neglecting the second target-cell population leads to underestimation of R_1 and R_2; consequently, drug levels determined from a one-target-cell model may be insufficient to clear the viruses. The model is extended to incorporate antiviral drug therapy and to determine the minimum drug efficacies required to eliminate viral coinfection. The results provide deeper insight into the dynamics of dual infections involving viruses that compete for distinct target-cell populations.

Keywords: coinfection; viral competition; Lyapunov method; global stability
Mathematics Subject Classification: 34D20, 34D23, 37N25, 92B05

1. Introduction

In recent decades, numerous human viruses have been identified, causing widespread illness and, in some cases, millions of deaths. Some of these viruses lead to chronic infections and are costly to treat, particularly those transmitted through bodily fluids, such as HIV-1, human T-cell lymphotropic virus type 1 (HTLV-1), hepatitis B/C virus (HBV/HCV). Other viruses are transmitted by mosquitoes and cause febrile illnesses, including Zika virus (ZIKV), dengue virus (DENV), and chikungunya virus (CHIKV). Respiratory viruses include influenza A virus (IAV) and the recently emerged SARS-CoV-2, the causative agent of coronavirus disease 2019 (COVID-19).

When a person is infected with two or more viruses, the condition is referred to as a viral coinfection. Some viruses share common transmission routes, such as HIV-1/HTLV-1 and HBV/HCV. Other examples include respiratory viruses and vector-borne viruses. Viral coinfections may also involve different strains of the same virus, such as SARS-CoV-2 (e.g., Delta and Omicron) [1], distinct HIV strains (e.g., HIV-1, and HIV-2) [2], DENV serotypes (DENV 1–4) [3] or multiple influenza virus strains. Because different viral infections can produce similar clinical symptoms, double viral infections are often difficult to diagnose and may increase disease severity. Accurate identification of such coinfections is therefore essential for effective clinical management and treatment.

Coinfection with HIV and HTLV-1 frequently occurs in regions where both viruses are endemic, particularly among populations exposed to high-risk behaviors such as unprotected sexual activity and needle sharing. These practices facilitate the exchange of infected bodily fluids, thereby increasing the likelihood of simultaneous transmission of the two viruses [4]. Injection drug use, unsafe healthcare procedures such as the reuse of contaminated needles, and unprotected sexual contact represent shared risk factors for both HCV and HBV infections, thereby raising the probability of coinfection [5]. HBV infection is frequently observed among individuals living with HIV, as both viruses share common routes of transmission, including blood transfusion, unprotected sexual contact, needle sharing, and mother-to-child transmission [6]. DENV, CHIKV, and ZIKV are transmitted to humans through the bites of infected female mosquitoes, primarily *Aedes aegypti* and *Aedes albopictus* [7]. IAV and SARS-CoV-2 spread among humans mainly through respiratory droplets [8].

1.1. Mathematical modeling context

Within-host viral dynamics can be effectively examined using mathematical modeling, which helps clarify how viruses interact with their susceptible host cells. An early and influential model in this field was proposed in [9], focusing on a single viral population such as HIV-1 that infects and reproduces within a single class of target cells, specifically $CD4^+$ T cells. The framework assumes that infection occurs when uninfected cells encounter free virus particles, a pathway known as virus-to-cell transmission.

In addition to infection mediated by free virus particles, many viruses are capable of spreading through direct cell-to-cell interactions, a pathway that has been shown to be considerably more effective than virus-to-cell transmission [10–12]. Viral infectivity may be further amplified through cytokine-enhanced mechanisms, which have been documented in HIV-1 infection. In cases where infection fails to complete, caspase-1-dependent pyroptosis is triggered, leading to inflammatory cell death accompanied by the release of proinflammatory cytokines [13]. The resulting inflammatory response recruits additional $CD4^+$ T cells to the affected tissue, thereby increasing susceptibility

to infection and subsequent pyroptosis, ultimately sustaining a self-reinforcing pathogenic cycle. Mathematical frameworks that incorporate cytokine-enhanced infection mechanisms have attracted increasing attention in recent years (see, for example, [14–16]). The original framework proposed in [9] has been generalized in numerous studies through the inclusion of additional biological mechanisms, such as intracellular time delays, delayed immune responses, and spatial diffusion effects (see, for instance, [17–19]).

Competition between two viruses for a shared target-cell population can be represented by the model proposed by [20]:

$$\dot{x} = \overbrace{\lambda}^{\text{recruitment of uninfected cells}} - \overbrace{dx}^{\text{death}} - \overbrace{\beta_1 x v_1}^{\text{infection driven by virus type 1}} - \overbrace{\beta_2 x v_2}^{\text{infection driven by virus type 2}}, \tag{1.1}$$

$$\dot{y}_1 = \overbrace{\beta_1 x v_1}^{\text{formation of virus-1-infected cells}} - \overbrace{a_1 y_1}^{\text{death}}, \tag{1.2}$$

$$\dot{y}_2 = \overbrace{\beta_2 x v_2}^{\text{formation of virus-2-infected cells}} - \overbrace{a_2 y_2}^{\text{death}}, \tag{1.3}$$

$$\dot{v}_1 = \overbrace{k_1 a_1 y_1}^{\text{release of virus type 1}} - \overbrace{c_1 v_1}^{\text{loss of free virus}}, \tag{1.4}$$

$$\dot{v}_2 = \overbrace{k_2 a_2 y_2}^{\text{release of virus type 2}} - \overbrace{c_2 v_2}^{\text{loss of free virus}}. \tag{1.5}$$

Here, $x = x(t)$, $y_i = y(t)$, and $v_i = v_i(t)$ represent the time-dependent concentrations of uninfected cells, infected cells, and free viruses, respectively, with $i = 1, 2$ denoting virus types 1 and 2. For SARS-CoV-2 coinfection with other respiratory viruses, including IAV, RSV, hRV, PIV, or hMPV, a target cell-limited model is typically used. The uninfected target-cell dynamics are described by [21]:

$$\dot{x} = -\beta_1 x v_1 - \beta_2 x v_2.$$

Model (1.1)–(1.5) exhibits three equilibria: the infection-free equilibrium, a virus-1 single-infection equilibrium, and a virus-2 single-infection equilibrium. Notably, the model does not permit a coexistence equilibrium. Extensions can produce coexistence states under specific biological conditions, such as:

(i) Superinfection, when one virus can invade cells already infected by another [22];

(ii) Immune interactions, where cytotoxic T lymphocytes (CTLs) or antibodies introduce regulatory feedback allowing both viruses to persist [23, 24];

(iii) Viral saturation effects, where nonlinear infection dynamics mitigate competition [25, 26]; and

(iv) Overlapping and distinct target cells, where one virus infects both shared and unique cell types [27, 28].

1.2. Examples of two-virus coinfection models

- SARS-CoV-2 and IAV: Dual infection models assume both viruses target the same cell type (epithelial cells) [21]. Elaiw et al. [29] examined antibody-mediated immune interactions, while Khumaeroh et al. [30] analyzed CTL-based immune dynamics.
- HIV-1 and HTLV-1: Several models [23, 31] describe coinfection within $CD4^+$ T cells (x_1), with HIV-1 also infecting macrophages (x_2). Other works introduced stochastic [32] and fractional-order [24] frameworks or saturated incidence dynamics [33].

- HIV-1 and HBV: Nampala et al. [27] modeled coinfection by assuming HBV infects hepatocytes (x_1) and that HIV-1 infects both hepatocytes (x_1) and CD4$^+$ T cells (x_2).
- HCV and HBV: Models with saturation and immune terms were developed in [25, 26], where both viruses target hepatocytes.
- Two viral strains: Coexistence of wild-type and mutant strains has been studied for HIV-1 and SARS-CoV-2 [34, 35]. Double-strain models for HCV [36] and HIV-1 [37–39] explore drug resistance and competition on shared targets (CD4$^+$ T cells). In these HIV-1 models, it is assumed that both drug-sensitive virus and drug-resistant virus are competing for the same target, CD4$^+$ T cells. Shi et al. [28] formulated a two-strain HIV-1 model by considering that both drug-sensitive virus and drug-resistant virus infect the same target, CD4$^+$ T cells; moreover, drug-sensitive have another target, macrophages.

Therefore, simultaneous competition of two viruses across multiple target-cell populations remains largely unexplored.

1.3. Target-cell diversity

There are documented cases where viruses replicate within multiple target-cell populations. For HIV-1 and HTLV-1, HIV-1 infects CD4$^+$ T cells, dendritic cells, and macrophages [40, 41]. HTLV-1 mainly targets CD4$^+$ T cells, but can also infect CD8$^+$ T cells, dendritic cells, and monocytes [42]. Regarding vector-borne viruses, several studies [43–45] have shown that DENV infects a variety of cell types, including monocytes, hepatocytes, macrophages, dendritic cells, and mast cells. CHIKV is transmitted through bites of infected mosquitoes and replicates in skeletal muscle satelliteOne major limitation of this study is the difficulty in accurately cells, fibroblasts, macrophages, monocytes, and skin cells [46, 47]. In addition, monocytes and dendritic cells are known to serve as major targets for ZIKV infection [48]. For hepatotropic viruses, both HBV and HCV infect hepatocytes but have also been found in peripheral blood mononuclear cells (PBMCs). These PBMCs are composed of lymphocytes (T cells, B cells, and natural killer cells) and monocytes, indicating possible extrahepatic replication [49–51].

Although many viruses preferentially infect a specific class of host cells, they may also invade and replicate within additional cell types. When multiple viruses are present in the host at the same time, overlapping cellular tropism can give rise to intricate coinfection dynamics, in which different viral agents compete across two or more populations of susceptible cells. Such interactions have been reported in several settings, including HIV-1/HTLV-1 coinfection, hepatitis virus coinfections, HIV-hepatitis combinations, mosquito-borne viral infections, and respiratory viruses. Despite this biological complexity, most existing coinfection models simplify the interaction by assuming a single shared target-cell population for both viruses. Under this assumption, the resulting dynamics primarily reflect viral competition rather than true coinfection. Genuine coinfection may instead arise through mechanisms such as cellular superinfection, evasion of adaptive immune responses, or limitations imposed by infection saturation.

The transmission potential and within-host dynamics of coinfecting viruses are influenced by several key factors. These include the abundance and diversity of target-cell populations, the efficiency of viral spread through both free virus and direct cell-to-cell pathways, immune-mediated regulation, and the extent to which viruses share or occupy distinct cell types. Accounting for these factors

provides a biological foundation for the model, shaping viral coexistence, competition outcomes, and the course and severity of infection. Explicit consideration of these elements enhances the relevance of the framework for understanding viral coinfections and guiding treatment strategies.

To our knowledge, no mathematical framework currently describes within-host dynamics in which two competing viruses (or strains) simultaneously infect two distinct target-cell populations. Motivated by these biological observations, we develop a model that allows each virus to infect both cell classes with different efficiencies. This structure permits coexistence driven solely by target-cell heterogeneity, without invoking superinfection, immune regulation, or saturation effects.

In this study, we formulate a within-host model for two competing viruses interacting across two target-cell populations. Explicit formulas for the basic reproduction numbers for single and dual infections are derived, and the global asymptotic stability of all equilibria is established using Lyapunov functions. The impact of secondary target-cell populations on long-term infection outcomes is examined, and numerical simulations are provided to support the analytical results and explore treatment effects. The proposed framework is applicable to a broad range of viral coinfections, including HIV-1/HTLV-1, hepatitis viruses, vector-borne infections, and respiratory pathogens.

2. Viral coinfection model

This section presents the formulation of a within-host coinfection system with two types of viruses, v_1 and v_2, interacting with two types of target cells, x_1 and x_2. Both viruses can infect either cell type, producing infected populations y_1, y_2 from x_1 and z_1, z_2 from x_2. Viruses are generated by infected cells, while natural cell turnover and viral clearance shape the dynamics. The viruses do not directly block each other but compete indirectly for the available uninfected target cells, affecting their replication within the host.

$$\dot{x}_1 = \lambda_1 - d_1 x_1 - \beta_1 x_1 v_1 - \beta_2 x_1 v_2, \tag{2.1}$$
$$\dot{y}_1 = \beta_1 x_1 v_1 - a_1 y_1, \tag{2.2}$$
$$\dot{y}_2 = \beta_2 x_1 v_2 - a_2 y_2, \tag{2.3}$$
$$\dot{x}_2 = \lambda_2 - d_2 x_2 - \beta_3 x_2 v_1 - \beta_4 x_2 v_2, \tag{2.4}$$
$$\dot{z}_1 = \beta_3 x_2 v_1 - a_3 z_1, \tag{2.5}$$
$$\dot{z}_2 = \beta_4 x_2 v_2 - a_4 z_2, \tag{2.6}$$
$$\dot{v}_1 = k_1 a_1 y_1 + k_3 a_3 z_1 - c_1 v_1, \tag{2.7}$$
$$\dot{v}_2 = k_2 a_2 y_2 + k_4 a_4 z_2 - c_2 v_2. \tag{2.8}$$

A description of all variables and parameters in the two-virus coinfection model is provided in Table 1. All model parameters are assumed to have positive values. The within-host infection pathways of the two viruses are depicted in Figure 1. The model is initialized with nonnegative starting values as follows:

$$x_1(0) > 0,\ y_1(0) \geq 0,\ y_2(0) \geq 0,\ x_2(0) > 0,\ z_1(0) \geq 0,\ z_2(0) \geq 0,\ v_1(0) \geq 0,\ v_2(0) \geq 0. \tag{2.9}$$

Table 1. Variables and parameters description of system (2.1)–(2.8).

Variable	Description
x_1	Target cells type 1
y_1	v_1-infected cells type 1
y_2	v_2-infected cells type 1
x_2	Target cells type 2
z_1	v_1-infected cells type 2
z_2	v_2-infected cells type 2
v_1	Virus particles type 1
v_2	Virus particles type 2
Parameter	**Description**
λ_1	Generation rate of target cells type 1, x_1
λ_2	Generation rate of target cells type 2, x_2
β_1	Incidence rate between virus particles type 1 and target cells type 1 (v_1 and x_1)
β_2	Incidence rate between virus particles type 2 and target cells type 1 (v_2 and x_1)
β_3	Incidence rate between virus particles type 1 and target cells type 2 (v_1 and x_2)
β_4	Incidence rate between virus particles type 2 and target cells type 2 (v_2 and x_2)
d_1	Mortality rate of target cells type 1
d_2	Mortality rate of target cells type 2
a_1	Mortality rate of v_1-infected cells type 1
a_2	Mortality rate of v_2-infected cells type 1
a_3	Mortality rate of v_1-infected cells type 2
a_4	Mortality rate of v_2-infected cells type 2
c_1	Destruction rate of virus particles type 1
c_2	Destruction rate of virus particles type 2
$k_i, i = 1, 2, 3, 4$	The average quantity of viral particles produced per infected cell during its lifespan

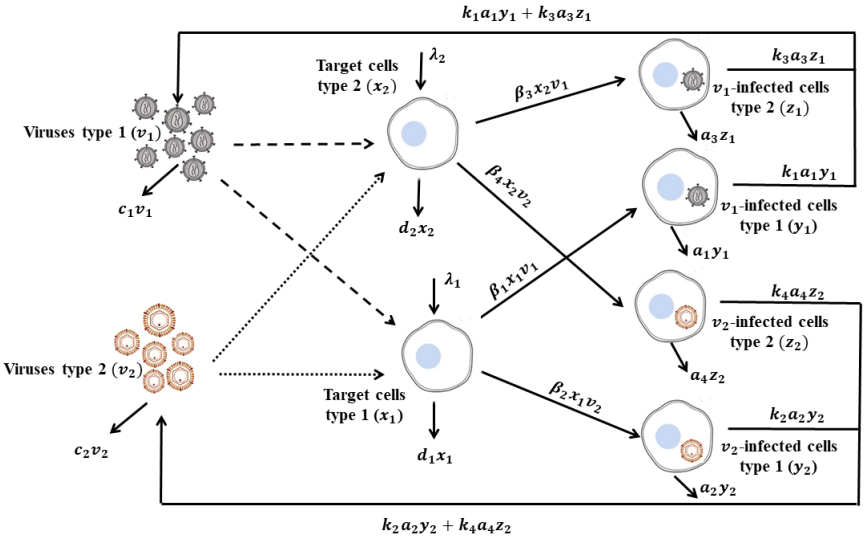

Figure 1. Diagrammatic representation of the within-host coinfection dynamics involving two viruses.

3. Well-posedness of solutions

The right-hand side of system (2.1)–(2.8) is continuous and satisfies the Lipschitz condition on the interval $[0, \delta]$, where $\delta > 0$. From the basic results of differential equation theory, the system (2.1)–(2.8) with nonnegative initial data (2.9) has a unique local solution $(x_1(t), y_1(t), y_2(t), x_2(t), z_1(t), z_2(t), v_1(t), v_2(t))$ for $t \in [0, t^*]$, where $0 < t^* < \infty$.

System (2.1)–(2.8) tracks cell and virus levels, which must stay nonnegative and finite. This is ensured by the lemma below.

Lemma 1. *The solutions of system (2.1)–(2.8) remain nonnegative and bounded.*

Proof. We find that

$$\begin{aligned}
&\dot{x}_1 \mid_{x_1=0} = \lambda_1 > 0,\\
&\dot{y}_1 \mid_{y_1=0} = \beta_1 x_1 v_1 \geq 0, \text{ for all } x_1, v_1 \geq 0,\\
&\dot{y}_2 \mid_{y_2=0} = \beta_2 x_1 v_2 \geq 0, \text{ for all } x_1, v_2 \geq 0,\\
&\dot{x}_2 \mid_{x_2=0} = \lambda_2 > 0,\\
&\dot{z}_1 \mid_{z_1=0} = \beta_3 x_2 v_1 \geq 0, \text{ for all } x_2, v_1 \geq 0,\\
&\dot{z}_2 \mid_{z_2=0} = \beta_4 x_2 v_2 \geq 0, \text{ for all } x_2, v_2 \geq 0,\\
&\dot{v}_1 \mid_{v_1=0} = k_1 a_1 y_1 + k_3 a_3 z_1 \geq 0, \text{ for all } y_1, z_1 \geq 0,\\
&\dot{v}_2 \mid_{v_2=0} = k_2 a_2 y_2 + k_4 a_4 z_2 \geq 0, \text{ for all } y_2, z_2 \geq 0.
\end{aligned}$$

Hence, by Proposition B.7 in [52], the solution $(x_1(t), y_1(t), y_2(t), x_2(t), z_1(t), z_2(t), v_1(t), v_2(t))$ remains in $\mathbb{R}^8_{\geq 0}$ for all $t \geq 0$, provided that the initial conditions $(x_1(0), y_1(0), y_2(0), x_2(0), z_1(0), z_2(0), v_1(0), v_2(0))$ belong to $\mathbb{R}^8_{\geq 0}$. Let us define $\Gamma = x_1 + y_1 + y_2 + x_2 + z_1 + z_2$. Then, we get

$$\begin{aligned}
\dot{\Gamma} &= \lambda_1 - d_1 x_1 - a_1 y_1 - a_2 y_2 + \lambda_2 - d_2 x_2 - a_3 z_1 - a_4 z_2\\
&\leq \lambda_1 + \lambda_2 - \sigma(x_1 + y_1 + y_2 + x_2 + z_1 + z_2) = \lambda_1 + \lambda_2 - \sigma\Gamma,
\end{aligned}$$

where $\sigma = \min\{d_1, d_2, a_1, a_2, a_3, a_4\}$. Hence, $0 \leq \Gamma(t) \leq \frac{\lambda_1+\lambda_2}{\sigma}$ for all $t \geq 0$ if $\Gamma(0) \leq \frac{\lambda_1+\lambda_2}{\sigma}$. This implies that $0 \leq x_1(t), y_1(t), y_2(t), x_2(t), z_1(t), z_2(t) \leq L_1$ if $0 \leq x_1(0) + y_1(0) + y_2(0) + x_2(0) + z_1(0) + z_2(0) \leq L_1$, where $L_1 = \frac{\lambda_1+\lambda_2}{\sigma}$. Moreover, From Eqs (2.7) and (2.8) we obtain

$$\begin{aligned}
\dot{v}_1 &= k_1 a_1 y_1 + k_3 a_3 z_1 - c_1 v_1 \leq k_1 a_1 L_1 + k_3 a_3 L_1 - c_1 v_1,\\
\dot{v}_2 &= k_2 a_2 y_2 + k_4 a_4 z_2 - c_2 v_2 \leq k_2 a_2 L_1 + k_4 a_4 L_1 - c_2 v_2.
\end{aligned}$$

It follows that $0 \leq v_1(t) \leq L_2$ if $0 \leq v_1(0) \leq L_2$, and $0 \leq v_2(t) \leq L_3$ if $0 \leq v_2(0) \leq L_3$, where $L_2 = \frac{1}{c_1}(k_1 a_1 L_1 + k_3 a_3 L_1)$ and $L_3 = \frac{1}{c_2}(k_2 a_2 L_1 + k_4 a_4 L_1)$. The compact set Δ defined by

$$\Delta = \left\{(x_1, y_1, y_2, x_2, z_1, z_2, v_1, v_2) \in \mathbb{R}^8_{\geq 0} : 0 \leq x_1, y_1, y_2, x_2, z_1, z_2 \leq L_1, 0 \leq v_1 \leq L_2, , 0 \leq v_2 \leq L_3\right\}$$

is positively invariant for system (2.1)–(2.8). □

4. Steady states analysis

Here, the model's steady states are explored and the corresponding existence criteria are derived. Any steady state $SS_i = (x_1, y_1, y_2, x_2, z_1, z_2, v_1, v_2)$ satisfies

$$0 = \lambda_1 - d_1 x_1 - \beta_1 x_1 v_1 - \beta_2 x_1 v_2, \tag{4.1}$$
$$0 = \beta_1 x_1 v_1 - a_1 y_1, \tag{4.2}$$
$$0 = \beta_2 x_1 v_2 - a_2 y_2, \tag{4.3}$$
$$0 = \lambda_2 - d_2 x_2 - \beta_3 x_2 v_1 - \beta_4 x_2 v_2, \tag{4.4}$$
$$0 = \beta_3 x_2 v_1 - a_3 z_1, \tag{4.5}$$
$$0 = \beta_4 x_2 v_2 - a_4 z_2, \tag{4.6}$$
$$0 = k_1 a_1 y_1 + k_3 a_3 z_1 - c_1 v_1, \tag{4.7}$$
$$0 = k_2 a_2 y_2 + k_4 a_4 z_2 - c_2 v_2. \tag{4.8}$$

Substituting Eqs (4.2), (4.3), (4.5), and (4.6) into Eqs (4.7) and (4.8), we obtain

$$(k_1\beta_1 x_1 + k_3\beta_3 x_2 - c_1)\, v_1 = 0, \tag{4.9}$$
$$(k_2\beta_2 x_1 + k_4\beta_4 x_2 - c_2)\, v_2 = 0. \tag{4.10}$$

Equations (4.9) and (4.10) provide the following cases:

Case 4.1. $v_1 = 0$ *and* $v_2 = 0$*:*

From Eqs (4.1)–(4.6), we get the infection-free steady state $SS_0 = \left(x_1^0, 0, 0, x_2^0, 0, 0, 0, 0\right)$, where $x_1^0 = \frac{\lambda_1}{d_1}$ and $x_2^0 = \frac{\lambda_2}{d_2}$.

By applying the next-generation matrix approach (see Appendix), we obtain

$$R_1 = R_{11} + R_{12} = \frac{k_1\beta_1\lambda_1}{c_1 d_1} + \frac{k_3\beta_3\lambda_2}{c_1 d_2},$$
$$R_2 = R_{21} + R_{22} = \frac{k_2\beta_2\lambda_1}{c_2 d_1} + \frac{k_4\beta_4\lambda_2}{c_2 d_2},$$
$$R_0 = \max\{R_1, R_2\}.$$

Here, R_1, R_2, and R_0 denote the basic reproduction numbers associated with infection by v_1 alone, v_2 alone, and their coinfection, respectively.

Case 4.2. $v_1 \neq 0$ *and* $v_2 = 0$*:*

From Eqs (4.1) and (4.4), we have

$$x_1 = \frac{\lambda_1}{d_1 + \beta_1 v_1}, \quad x_2 = \frac{\lambda_2}{d_2 + \beta_3 v_1}. \tag{4.11}$$

Substituting in Eq (4.9) we obtain

$$\frac{k_1\beta_1\lambda_1}{d_1 + \beta_1 v_1} + \frac{k_3\beta_3\lambda_2}{d_2 + \beta_3 v_1} - c_1 = 0,$$

which gives

$$\bar{A}v_1^2 + \bar{B}v_1 + \bar{C} = 0, \tag{4.12}$$

where

$$\begin{aligned}
&\bar{A} = c_1\beta_1\beta_3,\\
&\bar{B} = c_1d_2\beta_1 + c_1d_1\beta_3 - k_1\beta_1\beta_3\lambda_1 - k_3\beta_1\beta_3\lambda_2,\\
&\bar{C} = c_1d_1d_2 - d_2k_1\beta_1\lambda_1 - d_1k_3\beta_3\lambda_2 = -c_1d_1d_2\left(\frac{k_1\beta_1\lambda_1}{c_1d_1} + \frac{k_3\beta_3\lambda_2}{c_1d_2} - 1\right) = -c_1d_1d_2\,(R_1 - 1)\,.
\end{aligned}$$

We have $\bar{A} > 0$, and if $R_1 > 1$ then $\bar{C} < 0$ and Eq (4.12) has a unique positive root given by

$$\bar{v}_1 = \frac{-\bar{B} + \sqrt{\bar{B}^2 - 4\bar{A}\bar{C}}}{2\bar{A}}.$$

From Eqs (4.2), (4.5), and (4.11) we get

$$\bar{x}_1 = \frac{\lambda_1}{d_1 + \beta_1\bar{v}_1} > 0, \quad \bar{x}_2 = \frac{\lambda_2}{d_2 + \beta_3\bar{v}_1} > 0, \quad \bar{y}_1 = \frac{\beta_1\bar{x}_1\bar{v}_1}{a_1} > 0, \quad \bar{z}_1 = \frac{\beta_3\bar{x}_2\bar{v}_1}{a_3} > 0.$$

Therefore, an infected v_1-mono-infection steady state $SS_1 = (\bar{x}_1, \bar{y}_1, 0, \bar{x}_2, \bar{z}_1, 0, \bar{v}_1, 0)$ exists when R_1>1.

Case 4.3. $v_1 = 0$ *and* $v_2 \neq 0$*:*

From Eqs (4.1) and (4.4), we have

$$x_1 = \frac{\lambda_1}{d_1 + \beta_2v_2}, \quad x_2 = \frac{\lambda_2}{d_2 + \beta_4v_2}. \tag{4.13}$$

Substituting in Eq (4.10), we obtain

$$\frac{k_2\beta_2\lambda_1}{d_1 + \beta_2v_2} + \frac{k_4\beta_4\lambda_2}{d_2 + \beta_4v_2} - c_2 = 0,$$

which gives

$$A^*v_2^2 + B^*v_2 + C^* = 0, \tag{4.14}$$

where

$$\begin{aligned}
&A^* = c_2\beta_2\beta_4,\\
&B^* = c_2d_2\beta_2 + c_2d_1\beta_4 - k_2\beta_2\beta_4\lambda_1 - k_4\beta_2\beta_4\lambda_2,\\
&C^* = c_2d_1d_2 - d_2k_2\beta_2\lambda_1 - d_1k_4\beta_4\lambda_2 = -c_2d_1d_2\left(\frac{k_2\beta_2\lambda_1}{c_2d_1} + \frac{k_4\beta_4\lambda_2}{c_2d_2} - 1\right) = -c_2d_1d_2\,(R_2 - 1)\,.
\end{aligned}$$

We have $A^* > 0$, and if $R_2 > 1$ then $C^* < 0$ and Eq (4.14) has a unique positive root given by

$$v_2^* = \frac{-B^* + \sqrt{B^{*2} - 4A^*C^*}}{2A^*}.$$

From Eqs (4.3), (4.6), and (4.13), we get

$$x_1^* = \frac{\lambda_1}{d_1 + \beta_2v_2^*} > 0, \quad x_2^* = \frac{\lambda_2}{d_2 + \beta_4v_2^*} > 0, \quad y_2^* = \frac{\beta_2x_1^*v_2^*}{a_2} > 0, \quad z_2^* = \frac{\beta_4x_2^*v_2^*}{a_4} > 0.$$

Therefore, an infected v_2-mono-infection steady state $SS_2 = \left(x_1^*, 0, y_2^*, x_2^*, 0, z_2^*, 0, v_2^*\right)$ exists when R_2>1.

Case 4.4. *$v_1 \neq 0$ and $v_2 \neq 0$:*

In this case, we get a two-virus coexistence steady state $SS_3 = (\tilde{x}_1, \tilde{y}_1, \tilde{y}_2, \tilde{x}_2, \tilde{z}_1, \tilde{z}_2, \tilde{v}_1, \tilde{v}_2)$:

$$\tilde{x}_1 = \frac{c_1\left(\frac{R_{12}}{R_{22}} - 1\right)}{k_1\beta_1\left(\frac{R_{21}R_{12}}{R_{22}R_{11}} - 1\right)}, \qquad \tilde{x}_2 = \frac{c_2\left(\frac{R_{21}}{R_{11}} - 1\right)}{k_4\beta_4\left(\frac{R_{21}R_{12}}{R_{22}R_{11}} - 1\right)},$$

$$\tilde{y}_1 = \frac{\beta_1\tilde{x}_1\tilde{v}_1}{a_1}, \qquad \tilde{y}_2 = \frac{\beta_2\tilde{x}_1\tilde{v}_2}{a_2}, \qquad \tilde{z}_1 = \frac{\beta_3\tilde{x}_2\tilde{v}_1}{a_3}, \qquad \tilde{z}_2 = \frac{\beta_4\tilde{x}_2\tilde{v}_2}{a_4},$$

$$\tilde{v}_1 = \frac{d_1}{\beta_1}\frac{\gamma R_{11}\left(\frac{R_{21}R_{12}}{R_{22}R_{11}} - 1\right) + \left(\frac{R_{12}}{R_{22}} - 1\right)}{\gamma\left(\frac{R_{12}}{R_{22}} - 1\right)(R_3 - 1)}\left[\frac{\left(\frac{R_{12}}{R_{22}} - 1\right)\left\{R_{22}\left(\frac{R_{21}R_{12}}{R_{22}R_{11}} - 1\right) + \gamma\left(\frac{R_{21}}{R_{11}} - 1\right)\right\}}{\left(\frac{R_{21}}{R_{11}} - 1\right)\left\{\gamma R_{11}\left(\frac{R_{21}R_{12}}{R_{22}R_{11}} - 1\right) + \left(\frac{R_{12}}{R_{22}} - 1\right)\right\}} - 1\right],$$

$$\tilde{v}_2 = \frac{d_2}{\beta_4}\frac{R_{22}\left(\frac{R_{21}R_{12}}{R_{22}R_{11}} - 1\right) + \gamma R_3\left(\frac{R_{21}}{R_{11}} - 1\right)}{\left(\frac{R_{21}}{R_{11}} - 1\right)(R_3 - 1)}\left[\frac{\left(\frac{R_{21}}{R_{11}} - 1\right)\left\{\left(\frac{R_{12}}{R_{22}} - 1\right) + \gamma R_{11}R_3\left(\frac{R_{21}R_{12}}{R_{22}R_{11}} - 1\right)\right\}}{\left(\frac{R_{12}}{R_{22}} - 1\right)\left\{R_{22}\left(\frac{R_{21}R_{12}}{R_{22}R_{11}} - 1\right) + \gamma R_3\left(\frac{R_{21}}{R_{11}} - 1\right)\right\}} - 1\right],$$

where $\gamma = \frac{d_1\beta_4}{d_2\beta_2}$. The threshold $R_3 = \frac{\beta_2\beta_3}{\beta_1\beta_4}$ compares the cross-infection strengths of the two viruses across the two target-cell populations. Then SS_3 exists when the following conditions are satisfied:

$$\frac{R_{12}}{R_{22}} > 1, \ \frac{R_{21}}{R_{11}} > 1, \ R_3 > 1, \tag{C1}$$

$$\frac{\left(\frac{R_{12}}{R_{22}} - 1\right)\left\{R_{22}\left(\frac{R_{21}R_{12}}{R_{22}R_{11}} - 1\right) + \gamma\left(\frac{R_{21}}{R_{11}} - 1\right)\right\}}{\left(\frac{R_{21}}{R_{11}} - 1\right)\left\{\gamma R_{11}\left(\frac{R_{21}R_{12}}{R_{22}R_{11}} - 1\right) + \left(\frac{R_{12}}{R_{22}} - 1\right)\right\}} > 1, \tag{C2}$$

$$\frac{\left(\frac{R_{21}}{R_{11}} - 1\right)\left\{\left(\frac{R_{12}}{R_{22}} - 1\right) + \gamma R_{11}R_3\left(\frac{R_{21}R_{12}}{R_{22}R_{11}} - 1\right)\right\}}{\left(\frac{R_{12}}{R_{22}} - 1\right)\left\{R_{22}\left(\frac{R_{21}R_{12}}{R_{22}R_{11}} - 1\right) + \gamma R_3\left(\frac{R_{21}}{R_{11}} - 1\right)\right\}} > 1. \tag{C3}$$

From condition (C1) we have the following:

$$\frac{k_2\beta_2}{c_2} > \frac{k_1\beta_1}{c_1}, \ \frac{k_3\beta_3}{c_1} > \frac{k_4\beta_4}{c_2}, \text{ and } \frac{\beta_2\beta_3}{\beta_1\beta_4} > 1.$$

The condition $\frac{k_2\beta_2}{c_2} > \frac{k_1\beta_1}{c_1}$ indicates that virus type 2 replicates more efficiently than virus type 1 in the first target-cell population (x_1), producing a larger number of viable virions per unit time and gaining a competitive advantage that promotes its persistence and dominance in this niche. Similarly, $\frac{k_3\beta_3}{c_1} > \frac{k_4\beta_4}{c_2}$ shows that virus type 1 is more efficient in the second target-cell population (x_2), generating more surviving virions and allowing it to dominate this population, which acts as a refuge for virus type 1 even when virus type 2 is present elsewhere. The condition $\frac{\beta_2\beta_3}{\beta_1\beta_4} > 1$ reflects a complementary structure in which virus type 2 dominates x_1 (large β_2 relative to β_1) and virus type 1 dominates x_2 (large β_3 relative to β_4), representing niche partitioning. When these requirements are satisfied simultaneously, the intensity of direct competition is reduced, and each virus exhibits a preferential replication advantage in one target-cell population while remaining less effective in the other. This asymmetric replication pattern inhibits competitive exclusion and supports the stable persistence of both viral populations.

We note that although conditions (C2) and (C3) are necessary to ensure the coexistence of the two viral strains, their underlying biological interpretation is more nuanced.

The following lemma consolidates these findings:

Lemma 2. *The steady states of system (2.1)–(2.8) are characterized as follows:*

- *The infection-free steady state always exists, namely,*

$$SS_0 = (x_1^0, 0, 0, x_2^0, 0, 0, 0, 0).$$

- *If $R_1 > 1$, then an infected v_1-mono-infection steady state arises,*

$$SS_1 = (\bar{x}_1, \bar{y}_1, 0, \bar{x}_2, \bar{z}_1, 0, \bar{v}_1, 0),$$

  in addition to SS_0.
- *If $R_2 > 1$, then an infected v_2-mono-infection steady state appears,*

$$SS_2 = (x_1^*, 0, y_2^*, x_2^*, 0, z_2^*, 0, v_2^*),$$

  in addition to SS_0.
- *If conditions (C1)–(C3) hold, then a two-virus coexistence steady state is present,*

$$SS_3 = (\tilde{x}_1, \tilde{y}_1, \tilde{y}_2, \tilde{x}_2, \tilde{z}_1, \tilde{z}_2, \tilde{v}_1, \tilde{v}_2),$$

  together with SS_0, SS_1, and SS_2.

5. Global asymptotic stability

We employ a Lyapunov approach to analyze the global stability of the four steady states. Following the strategy used by [18, 53], we construct appropriate Lyapunov functions. For each $j = 0, 1, 2, 3$, let $\Theta_j(x_1, y_1, y_2, x_2, z_1, z_2, v_1, v_2)$ be a Lyapunov candidate, and define the set as

$$\Xi_j = \left\{(x_1, y_1, y_2, x_2, z_1, z_2, v_1, v_2) : \frac{d\Theta_j}{dt} = 0\right\}.$$

Denote by Ξ_j' the largest invariant subset of Ξ_j. The following arithmetic–geometric mean inequality will be repeatedly used:

$$\sqrt[m]{\prod_{j=1}^{m} s_j} \leq \frac{1}{m}\sum_{j=1}^{m} s_j, \qquad s_j \geq 0, \quad j = 1, 2, ... \tag{5.1}$$

To simplify the global stability analysis, we assume $k_{13} = k_1 = k_3$ (and similarly $k_{24} = k_2 = k_4$). Biologically, this corresponds to the scenario in which each virus produces a similar number of virions per infected cell, regardless of whether the infection occurs in the primary or secondary target-cell population. This assumption does not affect the qualitative dynamics but allows for the derivation of analytical Lyapunov functions and the establishment of global stability results.

Theorem 1. *If $R_0 = \max\{R_1, R_2\} \leq 1$, then $SS_0 = (x_1^0, 0, 0, x_2^0, 0, 0, 0, 0)$ is globally asymptotically stable (G.A.S), otherwise it is unstable.*

Proof. Formulate a Lyapunov function Θ_0 as:

$$\Theta_0 = x_1^0\left(\frac{x_1}{x_1^0} - 1 - \ln\frac{x_1}{x_1^0}\right) + y_1 + y_2 + x_2^0\left(\frac{x_2}{x_2^0} - 1 - \ln\frac{x_2}{x_2^0}\right) + z_1 + z_2 + \frac{1}{k_{13}}v_1 + \frac{1}{k_{24}}v_2.$$

Calculate $\frac{d\Theta_0}{dt}$ along the solutions of model (2.1)–(2.8) as:

$$\begin{aligned}\frac{d\Theta_0}{dt} =& \left(1 - \frac{x_1^0}{x_1}\right)(\lambda_1 - d_1x_1 - \beta_1x_1v_1 - \beta_2x_1v_2) + \beta_1x_1v_1 - a_1y_1\\ &+ \beta_2x_1v_2 - a_2y_2 + \left(1 - \frac{x_2^0}{x_2}\right)(\lambda_2 - d_2x_2 - \beta_3x_2v_1 - \beta_4x_2v_2) + \beta_3x_2v_1 - a_3z_1\\ &+ \beta_4x_2v_2 - a_4z_2 + \frac{1}{k_{13}}(k_{13}a_1y_1 + k_{13}a_3z_1 - c_1v_1)\\ &+ \frac{1}{k_{24}}(k_{24}a_2y_2 + k_{24}a_4z_2 - c_2v_2)\\ =& \left(1 - \frac{x_1^0}{x_1}\right)(\lambda_1 - d_1x_1) + \left(1 - \frac{x_2^0}{x_2}\right)(\lambda_2 - d_2x_2) + \beta_1x_1^0v_1 + \beta_2x_1^0v_2\\ &+ \beta_3x_2^0v_1 + \beta_4x_2^0v_2 - \frac{c_1}{k_{13}}v_1 - \frac{c_2}{k_{24}}v_2.\end{aligned}$$

Substituting $\lambda_1 = d_1x_1^0$ and $\lambda_2 = d_2x_2^0$, we obtain

$$\frac{d\Theta_0}{dt} = -d_1\frac{(x_1 - x_1^0)^2}{x_1} - d_2\frac{(x_2 - x_2^0)^2}{x_2} + \frac{c_1}{k_{13}}(R_1 - 1)v_1 + \frac{c_2}{k_{24}}(R_2 - 1)v_2.$$

Therefore, for all $x_1, y_1, y_2, x_2, z_1, z_2, v_1, v_2 > 0$ we have $\frac{d\Theta_0}{dt} \le 0$. Moreover, $\frac{d\Theta_0}{dt} = 0$ when $x_1 = x_1^0$, $x_2 = x_2^0$, and $v_1 = v_2 = 0$. The solutions of system (2.1)–(2.8) tend to Ξ_0', which contains elements that satisfy $x_1(t) = x_1^0$, $x_2(t) = x_2^0$, and $v_1(t) = v_2(t) = 0$ [54]. Hence, $\dot{v}_1(t) = \dot{v}_2(t) = 0$, and from Eqs (2.7) and (2.8), we have

$$\begin{aligned}0 &= k_1a_1y_1(t) + k_3a_3z_1(t),\\ 0 &= k_2a_2y_2(t) + k_4a_4z_2(t),\end{aligned}$$

which leads to $y_1(t) = y_2(t) = z_1(t) = z_2(t) = 0$ for all t, and hence $\Xi_0' = \{SS_0\}$. LaSalle's invariance principle (L.I.P.) reveals that SS_0 is G.A.S [55].

To prove that SS_0 is unstable when $R_0 > 1$, the Jacobian matrix $J = J(x_1, y_1, y_2, x_2, z_1, z_2, v_1, v_2)$ of model (2.1)–(2.8) is calculated as:

$$J = \begin{pmatrix} -(d_1 + \beta_1v_1 + \beta_2v_2) & 0 & 0 & 0 & 0 & 0 & -\beta_1x_1 & -\beta_2x_1\\ \beta_1v_1 & -a_1 & 0 & 0 & 0 & 0 & \beta_1x_1 & 0\\ \beta_2v_2 & 0 & -a_2 & 0 & 0 & 0 & 0 & \beta_2x_1\\ 0 & 0 & 0 & -(d_2 + \beta_3v_1 + \beta_4v_2) & 0 & 0 & -\beta_3x_2 & -\beta_4x_2\\ 0 & 0 & 0 & \beta_3v_1 & -a_3 & 0 & \beta_3x_2 & 0\\ 0 & 0 & 0 & \beta_4v_2 & 0 & -a_4 & 0 & \beta_4x_2\\ 0 & k_{13}a_1 & 0 & 0 & k_{13}a_3 & 0 & -c_1 & 0\\ 0 & 0 & k_{24}a_2 & 0 & 0 & k_{24}a_4 & 0 & -c_2 \end{pmatrix}. \quad (5.2)$$

We calculate the characteristic equation at the equilibrium SS_0 as:

$$(\xi + d_1)(\xi + d_2)\left(\xi^3 + A_2\xi^2 + A_1\xi + A_0\right)\left(\xi^3 + B_2\xi^2 + B_1\xi + B_0\right) = 0, \tag{5.3}$$

where ξ is the eigenvalue and

$$\begin{aligned}
A_2 &= a_1 + a_3 + c_1,\\
A_1 &= a_1a_3 + a_1c_1 + a_3c_1 - \frac{a_1k_{13}\beta_1\lambda_1}{d_1} - \frac{a_3k_{13}\beta_3\lambda_2}{d_2},\\
A_0 &= a_1a_3c_1\left(1 - R_1\right),\\
B_2 &= a_2 + a_4 + c_2,\\
B_1 &= a_2a_4 + a_2c_2 + a_4c_2 - \frac{a_2k_{24}\beta_2\lambda_1}{d_1} - \frac{a_4k_{24}\beta_4\lambda_2}{d_2},\\
B_0 &= a_2a_4c_2\left(1 - R_2\right).
\end{aligned}$$

Clearly, if $R_1 > 1$ and/or $R_2 > 1$, then $A_0 < 0$ and/or $B_0 < 0$; Therefore Eq (5.3) has a positive root, and hence SS_0 is unstable. □

When both reproduction numbers satisfy $R_1, R_2 \leq 1$, the infections are predicted to disappear over time, regardless of the initial infection levels or disease state. Under these conditions, neither virus can persist within the host, leading to complete clearance and recovery of the target-cell populations.

Theorem 2. *If $R_1 > 1$ and $R_2 \leq 1$, then $SS_1 = (\bar{x}_1, \bar{y}_1, 0, \bar{x}_2, \bar{z}_1, 0, \bar{v}_1, 0)$ is G.A.S.*

Proof. Consider a function:

$$\begin{aligned}
\Theta_1 =& \bar{x}_1\left(\frac{x_1}{\bar{x}_1} - 1 - \ln\frac{x_1}{\bar{x}_1}\right) + \bar{y}_1\left(\frac{y_1}{\bar{y}_1} - 1 - \ln\frac{y_1}{\bar{y}_1}\right) + y_2 + \bar{x}_2\left(\frac{x_2}{\bar{x}_2} - 1 - \ln\frac{x_2}{\bar{x}_2}\right)\\
&+ \bar{z}_1\left(\frac{z_1}{\bar{z}_1} - 1 - \ln\frac{z_1}{\bar{z}_1}\right) + z_2 + \frac{\bar{v}_1}{k_{13}}\left(\frac{v_1}{\bar{v}_1} - 1 - \ln\frac{v_1}{\bar{v}_1}\right) + \frac{1}{k_{24}}v_2.
\end{aligned}$$

Calculate $\frac{d\Theta_1}{dt}$ as:

$$\begin{aligned}
\frac{d\Theta_1}{dt} =& \left(1 - \frac{\bar{x}_1}{x_1}\right)(\lambda_1 - d_1x_1 - \beta_1x_1v_1 - \beta_2x_1v_2) + \left(1 - \frac{\bar{y}_1}{y_1}\right)(\beta_1x_1v_1 - a_1y_1)\\
&+ \beta_2x_1v_2 - a_2y_2 + \left(1 - \frac{\bar{x}_2}{x_2}\right)(\lambda_2 - d_2x_2 - \beta_3x_2v_1 - \beta_4x_2v_2)\\
&+ \left(1 - \frac{\bar{z}_1}{z_1}\right)(\beta_3x_2v_1 - a_3z_1) + \beta_4x_2v_2 - a_4z_2\\
&+ \frac{1}{k_{13}}\left(1 - \frac{\bar{v}_1}{v_1}\right)(k_{13}a_1y_1 + k_{13}a_3z_1 - c_1v_1) + \frac{1}{k_{24}}(k_{24}a_2y_2 + k_{24}a_4z_2 - c_2v_2)\\
=& \left(1 - \frac{\bar{x}_1}{x_1}\right)(\lambda_1 - d_1x_1) + \beta_1\bar{x}_1v_1 + \beta_2\bar{x}_1v_2 - \frac{\beta_1x_1v_1\bar{y}_1}{y_1} + a_1\bar{y}_1\\
&+ \left(1 - \frac{\bar{x}_2}{x_2}\right)(\lambda_2 - d_2x_2) + \beta_3\bar{x}_2v_1 + \beta_4\bar{x}_2v_2 - \frac{\beta_3x_2v_1\bar{z}_1}{z_1} + a_3\bar{z}_1
\end{aligned}$$

$$-\frac{c_1}{k_{13}}v_1 - a_1\frac{y_1\bar{v}_1}{v_1} - a_3\frac{z_1\bar{v}_1}{v_1} + \frac{c_1}{k_{13}}\bar{v}_1 - \frac{c_2}{k_{24}}v_2.$$

Use the steady state conditions for SS_1:

$$\begin{aligned}
&\lambda_1 = d_1\bar{x}_1 + \beta_1\bar{x}_1\bar{v}_1, \qquad && \lambda_2 = d_2\bar{x}_2 + \beta_3\bar{x}_2\bar{v}_1,\\
&a_1\bar{y}_1 = \beta_1\bar{x}_1\bar{v}_1, && a_3\bar{z}_1 = \beta_3\bar{x}_2\bar{v}_1,\\
&c_1\bar{v}_1 = k_{13}\left(a_1\bar{y}_1 + a_3\bar{z}_1\right).
\end{aligned}$$

Then, we have

$$\begin{aligned}
\frac{d\Theta_1}{dt} =& \left(1-\frac{\bar{x}_1}{x_1}\right)(d_1\bar{x}_1 + a_1\bar{y}_1 - d_1x_1) - a_1\bar{y}_1\frac{x_1v_1\bar{y}_1}{\bar{x}_1\bar{v}_1y_1} + 2a_1\bar{y}_1 + \left(1-\frac{\bar{x}_2}{x_2}\right)(d_2\bar{x}_2 + a_3\bar{z}_1 - d_2x_2)\\
&- a_3\bar{z}_1\frac{x_2v_1\bar{z}_1}{\bar{x}_2\bar{v}_1z_1} + 2a_3\bar{z}_1 - a_1\bar{y}_1\frac{y_1\bar{v}_1}{\bar{y}_1v_1} - a_3\bar{z}_1\frac{z_1\bar{v}_1}{\bar{z}_1v_1} + \left(\beta_2\bar{x}_1 + \beta_4\bar{x}_2 - \frac{c_2}{k_{24}}\right)v_2\\
=& -d_1\frac{(x_1-\bar{x}_1)^2}{x_1} - d_2\frac{(x_2-\bar{x}_2)^2}{x_2} + a_1\bar{y}_1\left(3 - \frac{\bar{x}_1}{x_1} - \frac{x_1v_1\bar{y}_1}{\bar{x}_1\bar{v}_1y_1} - \frac{y_1\bar{v}_1}{\bar{y}_1v_1}\right)\\
&+ a_3\bar{z}_1\left(3 - \frac{\bar{x}_2}{x_2} - \frac{x_2v_1\bar{z}_1}{\bar{x}_2\bar{v}_1z_1} - \frac{z_1\bar{v}_1}{\bar{z}_1v_1}\right) + \left(\frac{\beta_2\lambda_1}{d_1+\beta_1\bar{v}_1} + \frac{\beta_4\lambda_2}{d_2+\beta_3\bar{v}_1} - \frac{c_2}{k_{24}}\right)v_2. \qquad (5.4)
\end{aligned}$$

Since $\bar{v}_1 > 0$, then we have

$$\left(\frac{\beta_2\lambda_1}{d_1+\beta_1\bar{v}_1} + \frac{\beta_4\lambda_2}{d_2+\beta_3\bar{v}_1} - \frac{c_2}{k_{24}}\right)v_2 \le \left(\frac{\beta_2\lambda_1}{d_1} + \frac{\beta_4\lambda_2}{d_2} - \frac{c_2}{k_{24}}\right)v_2 = \frac{c_2}{k_{24}}\left(\frac{\beta_2k_{24}\lambda_1}{c_2d_1} + \frac{\beta_4k_{24}\lambda_2}{c_2d_2} - 1\right)v_2 = \frac{c_2}{k_{24}}\left(R_2 - 1\right)v_2.$$

Therefore, Eq (5.4) takes the following form:

$$\begin{aligned}
\frac{d\Theta_1}{dt} \le& -d_1\frac{(x_1-\bar{x}_1)^2}{x_1} - d_2\frac{(x_2-\bar{x}_2)^2}{x_2} + a_1\bar{y}_1\left(3 - \frac{\bar{x}_1}{x_1} - \frac{x_1v_1\bar{y}_1}{\bar{x}_1\bar{v}_1y_1} - \frac{y_1\bar{v}_1}{\bar{y}_1v_1}\right)\\
&+ a_3\bar{z}_1\left(3 - \frac{\bar{x}_2}{x_2} - \frac{x_2v_1\bar{z}_1}{\bar{x}_2\bar{v}_1z_1} - \frac{z_1\bar{v}_1}{\bar{z}_1v_1}\right) + \frac{c_2}{k_{24}}\left(R_2 - 1\right)v_2.
\end{aligned}$$

If $R_2 \le 1$, then using inequality (5.1), we obtain $\frac{d\Theta_1}{dt} \le 0$ for all $x_1, y_1, y_2, x_2, z_1, z_2, v_1, v_2 > 0$. Moreover, $\frac{d\Theta_1}{dt} = 0$ occurs at $x_1 = \bar{x}_1$, $x_2 = \bar{x}_2$, $y_1 = \bar{y}_1$, $z_1 = \bar{z}_1$, $v_1 = \bar{v}_1$, and $v_2 = 0$. The solutions of the system tend to Ξ_1', which contains elements that satisfy $x_1(t) = \bar{x}_1$, $x_2(t) = \bar{x}_2$, $y_1(t) = \bar{y}_1$, $z_1(t) = \bar{z}_1$, $v_1(t) = \bar{v}_1$, and $v_2(t) = 0$. Hence $\dot{v}_2(t) = 0$, and from Eq (2.8), we have

$$0 = \dot{v}_2(t) = k_2a_2y_2(t) + k_4a_4z_2(t),$$

which leads to $y_2(t) = z_2(t) = 0$ for all t, and hence $\Xi_1' = \{SS_1\}$. LaSalle's invariance principle (L.I.P.) reveals that SS_1 is G.A.S. □

Theorem 3. *If $R_2 > 1$ and $R_1 \le 1$, then $SS_2 = \left(x_1^*, 0, y_2^*, x_2^*, 0, z_2^*, 0, v_2^*\right)$ is G.A.S.*

Proof. Let us formulate a function Θ_1 as:

$$\Theta_2 = x_1^*\left(\frac{x_1}{x_1^*} - 1 - \ln\frac{x_1}{x_1^*}\right) + y_1 + y_2^*\left(\frac{y_2}{y_2^*} - 1 - \ln\frac{y_2}{y_2^*}\right) + x_2^*\left(\frac{x_2}{x_2^*} - 1 - \ln\frac{x_2}{x_2^*}\right)$$

$$+ z_1 + z_2^*\left(\frac{z_2}{z_2^*} - 1 - \ln\frac{z_2}{z_2^*}\right) + \frac{1}{k_{13}}v_1 + \frac{v_2^*}{k_{24}}\left(\frac{v_2}{v_2^*} - 1 - \ln\frac{v_2}{v_2^*}\right).$$

Calculate $\frac{d\Theta_2}{dt}$ along the solutions of model (2.1)–(2.8) as:

$$\begin{aligned}
\frac{d\Theta_2}{dt} =& \left(1 - \frac{x_1^*}{x_1}\right)(\lambda_1 - d_1x_1 - \beta_1x_1v_1 - \beta_2x_1v_2) + \beta_1x_1v_1 - a_1y_1 \\
&+ \left(1 - \frac{y_2^*}{y_2}\right)(\beta_2x_1v_2 - a_2y_2) + \left(1 - \frac{x_2^*}{x_2}\right)(\lambda_2 - d_2x_2 - \beta_3x_2v_1 - \beta_4x_2v_2) \\
&+ \beta_3x_2v_1 - a_3z_1 + \left(1 - \frac{z_2^*}{z_2}\right)(\beta_4x_2v_2 - a_4z_2) \\
&+ \frac{1}{k_{13}}(k_{13}a_1y_1 + k_{13}a_3z_1 - c_1v_1) + \frac{1}{k_{24}}\left(1 - \frac{v_2^*}{v_2}\right)(k_{24}a_2y_2 + k_{24}a_4z_2 - c_2v_2) \\
=& \left(1 - \frac{x_1^*}{x_1}\right)(\lambda_1 - d_1x_1) + \beta_1x_1^*v_1 + \beta_2x_1^*v_2 - \frac{\beta_2x_1v_2y_2^*}{y_2} + a_2y_2^* \\
&+ \left(1 - \frac{x_2^*}{x_2}\right)(\lambda_2 - d_2x_2) + \beta_3x_2^*v_1 + \beta_4x_2^*v_2 - \frac{\beta_4x_2v_2z_2^*}{z_2} + a_4z_2^* \\
&- \frac{c_1}{k_{13}}v_1 - \frac{c_2}{k_{24}}v_2 - a_2\frac{y_2v_2^*}{v_2} - a_4\frac{z_2v_2^*}{v_2} + \frac{c_2}{k_{24}}v_2^*.
\end{aligned}$$

Utilize the following conditions for SS_2:

$$\begin{aligned}
&\lambda_1 = d_1x_1^* + \beta_2x_1^*v_2^*, \qquad &&\lambda_2 = d_2x_2^* + \beta_4x_2^*v_2^*, \\
&a_2y_2^* = \beta_2x_1^*v_2^*, &&a_4z_2^* = \beta_4x_2^*v_2^*, \\
&c_2v_2^* = k_{24}\left(a_2y_2^* + a_4z_2^*\right).
\end{aligned}$$

Then, we get

$$\begin{aligned}
\frac{d\Theta_2}{dt} =& \left(1 - \frac{x_1^*}{x_1}\right)(d_1x_1^* + a_2y_2^* - d_1x_1) - a_2y_2^*\frac{x_1v_2y_2^*}{x_1^*v_2^*y_2} + 2a_2y_2^* + \left(1 - \frac{x_2^*}{x_2}\right)(d_2x_2^* + a_4z_2^* - d_2x_2) \\
&- a_4z_2^*\frac{x_2v_2z_2^*}{x_2^*v_2^*z_2} + 2a_4z_2^* - a_2y_2^*\frac{y_2v_2^*}{y_2^*v_2} - a_4z_2^*\frac{z_2v_2^*}{z_2^*v_2} + (\beta_1x_1^* + \beta_3x_2^* - \frac{c_1}{k_{13}})v_1 \\
=& - d_1\frac{(x_1 - x_1^*)^2}{x_1} - d_2\frac{(x_2 - x_2^*)^2}{x_2} + a_2y_2^*\left(3 - \frac{x_1^*}{x_1} - \frac{x_1v_2y_2^*}{x_1^*v_2^*y_2} - \frac{y_2v_2^*}{y_2^*v_2}\right) \\
&+ a_4z_2^*\left(3 - \frac{x_2^*}{x_2} - \frac{x_2v_2z_2^*}{x_2^*v_2^*z_2} - \frac{z_2v_2^*}{z_2^*v_2}\right) + (\frac{\beta_1\lambda_1}{d_1 + \beta_2v_2^*} + \frac{\beta_3\lambda_2}{d_2 + \beta_4v_2^*} - \frac{c_1}{k_{13}})v_1.
\end{aligned}$$

Since $v_2^* > 0$, then

$$\left(\frac{\beta_1\lambda_1}{d_1+\beta_2v_2^*} + \frac{\beta_3\lambda_2}{d_2+\beta_4v_2^*} - \frac{c_1}{k_{13}}\right)v_1 \le \left(\frac{\beta_1\lambda_1}{d_1} + \frac{\beta_3\lambda_2}{d_2} - \frac{c_1}{k_{13}}\right)v_1 = \frac{c_1}{k_{13}}\left(\frac{\beta_1k_{13}\lambda_1}{d_1c_1} + \frac{\lambda_2k_{13}\beta_3}{d_2c_1} - 1\right)v_1 = \frac{c_1}{k_{13}}\left(R_1 - 1\right)v_1.$$

Therefore, we obtain

$$\frac{d\Theta_2}{dt} \le - d_1\frac{(x_1 - x_1^*)^2}{x_1} - d_2\frac{(x_2 - x_2^*)^2}{x_2} + a_2y_2^*\left(3 - \frac{x_1^*}{x_1} - \frac{x_1v_2y_2^*}{x_1^*v_2^*y_2} - \frac{y_2v_2^*}{y_2^*v_2}\right)$$

$$+ a_4 z_2^* \left(3 - \frac{x_2^*}{x_2} - \frac{x_2 v_2 z_2^*}{x_2^* v_2^* z_2} - \frac{z_2 v_2^*}{z_2^* v_2}\right) + \frac{c_1}{k_{13}} (R_1 - 1) v_1.$$

If $R_1 \leq 1$, then using inequality (5.1) we get $\frac{d\Theta_2}{dt} \leq 0$ for all $x_1, y_1, y_2, x_2, z_1, z_2, v_1, v_2 > 0$ and $\frac{d\Theta_2}{dt} = 0$ when $x_1 = x_1^*, y_2 = y_2^*, x_2 = x_2^*, z_2 = z_2^*, v_2 = v_2^*$ and $v_1 = 0$. The solutions of the system tend to Ξ_2', which contains elements that satisfy $x_1(t) = x_1^*, y_2(t) = y_2^*, x_2(t) = x_2^*, z_2(t) = z_2^*, v_2(t) = v_2^*$, and $v_1(t) = 0$. Then, from Eq (2.7), we get

$$0 = \dot{v}_1(t) = k_1 a_1 y_1(t) + k_3 a_3 z_1(t),$$

which gives $y_1(t) = z_1(t) = 0$ for all t. Hence, $\Xi_2' = \{SS_2\}$, and then L.I.P. implies that SS_2 is G.A.S. □

If one virus has a reproduction number above 1 while the other remains below 1, the virus with the higher R_i establishes a stable infection, and the other virus is eliminated, regardless of the initial infection levels or disease state. These equilibria reflect competitive exclusion, where the surviving virus determines the infection dynamics.

Theorem 4. *Suppose that conditions (C1)–(C3) are satisfied, then $SS_3 = (\tilde{x}_1, \tilde{y}_1, \tilde{y}_2, \tilde{x}_2, \tilde{z}_1, \tilde{z}_2, \tilde{v}_1, \tilde{v}_2)$ is G.A.S.*

Proof. Define

$$\begin{aligned}\Theta_3 =& \tilde{x}_1 \left(\frac{x_1}{\tilde{x}_1} - 1 - \ln \frac{x_1}{\tilde{x}_1}\right) + \tilde{y}_1 \left(\frac{y_1}{\tilde{y}_1} - 1 - \ln \frac{y_1}{\tilde{y}_1}\right) + \tilde{y}_2 \left(\frac{y_2}{\tilde{y}_2} - 1 - \ln \frac{y_2}{\tilde{y}_2}\right) + \tilde{x}_2 \left(\frac{x_2}{\tilde{x}_2} - 1 - \ln \frac{x_2}{\tilde{x}_2}\right) \\ &+ \tilde{z}_1 \left(\frac{z_1}{\tilde{z}_1} - 1 - \ln \frac{z_1}{\tilde{z}_1}\right) + \tilde{z}_2 \left(\frac{z_2}{\tilde{z}_2} - 1 - \ln \frac{z_2}{\tilde{z}_2}\right) + \frac{\tilde{v}_1}{k_{13}} \left(\frac{v_1}{\tilde{v}_1} - 1 - \ln \frac{v_1}{\tilde{v}_1}\right) + \frac{\tilde{v}_2}{k_{24}} \left(\frac{v_2}{\tilde{v}_2} - 1 - \ln \frac{v_2}{\tilde{v}_2}\right).\end{aligned}$$

Calculate $\frac{d\Theta_3}{dt}$ as:

$$\begin{aligned}\frac{d\Theta_3}{dt} =& \left(1 - \frac{\tilde{x}_1}{x_1}\right)(\lambda_1 - d_1 x_1 - \beta_1 x_1 v_1 - \beta_2 x_1 v_2) + \left(1 - \frac{\tilde{y}_1}{y_1}\right)(\beta_1 x_1 v_1 - a_1 y_1) \\ &+ \left(1 - \frac{\tilde{y}_2}{y_2}\right)(\beta_2 x_1 v_2 - a_2 y_2) + \left(1 - \frac{\tilde{x}_2}{x_2}\right)(\lambda_2 - d_2 x_2 - \beta_3 x_2 v_1 - \beta_4 x_2 v_2) \\ &+ \left(1 - \frac{\tilde{z}_1}{z_1}\right)(\beta_3 x_2 v_1 - a_3 z_1) + \left(1 - \frac{\tilde{z}_2}{z_2}\right)(\beta_4 x_2 v_2 - a_4 z_2) \\ &+ \frac{1}{k_{13}} \left(1 - \frac{\tilde{v}_1}{v_1}\right)(k_{13} a_1 y_1 + k_{13} a_3 z_1 - c_1 v_1) + \frac{1}{k_{24}} \left(1 - \frac{\tilde{v}_2}{v_2}\right)(k_{24} a_2 y_2 + k_{24} a_4 z_2 - c_2 v_2) \\ =& \left(1 - \frac{\tilde{x}_1}{x_1}\right)(\lambda_1 - d_1 x_1) + \beta_1 \tilde{x}_1 v_1 + \beta_2 \tilde{x}_1 v_2 - \frac{\beta_1 x_1 v_1 \tilde{y}_1}{y_1} + a_1 \tilde{y}_1 \\ &- \frac{\beta_2 x_1 v_2 \tilde{y}_2}{y_2} + a_2 \tilde{y}_2 + \left(1 - \frac{\tilde{x}_2}{x_2}\right)(\lambda_2 - d_2 x_2) + \beta_3 \tilde{x}_2 v_1 + \beta_4 \tilde{x}_2 v_2 \\ &- \frac{\beta_3 x_2 v_1 \tilde{z}_1}{z_1} + a_3 \tilde{z}_1 - \frac{\beta_4 x_2 v_2 \tilde{z}_2}{z_2} + a_4 \tilde{z}_2 - \frac{c_1}{k_{13}} v_1 - a_1 \frac{y_1 \tilde{v}_1}{v_1} - a_3 \frac{z_1 \tilde{v}_1}{v_1} \\ &+ \frac{c_1}{k_{13}} \tilde{v}_1 - \frac{c_2}{k_{24}} v_2 - a_2 \frac{y_2 \tilde{v}_2}{v_2} - a_4 \frac{z_2 \tilde{v}_2}{v_2} + \frac{c_2}{k_{24}} \tilde{v}_2.\end{aligned}$$

Use the steady state conditions for SS_3:

$$\begin{aligned}
&\lambda_1 = d_1\tilde{x}_1 + \beta_1\tilde{x}_1\tilde{v}_1 + \beta_2\tilde{x}_1\tilde{v}_2, \qquad \lambda_2 = d_2\tilde{x}_2 + \beta_3\tilde{x}_2\tilde{v}_1 + \beta_4\tilde{x}_2\tilde{v}_2,\\
&a_1\tilde{y}_1 = \beta_1\tilde{x}_1\tilde{v}_1, \quad a_2\tilde{y}_2 = \beta_2\tilde{x}_1\tilde{v}_2, \quad a_3\tilde{z}_1 = \beta_3\tilde{x}_2\tilde{v}_1, \quad a_4\tilde{z}_2 = \beta_4\tilde{x}_2\tilde{v}_2,\\
&c_1\tilde{v}_1 = k_{13}\left(a_1\tilde{y}_1 + a_3\tilde{z}_1\right), \qquad c_1\tilde{v}_2 = k_{24}\left(a_2\tilde{y}_2 + a_4\tilde{z}_2\right).
\end{aligned}$$

Then, we get

$$\begin{aligned}
\frac{d\Theta_3}{dt} =& \left(1 - \frac{\tilde{x}_1}{x_1}\right)(d_1\tilde{x}_1 + a_1\tilde{y}_1 + a_2\tilde{y}_2 - d_1x_1) - a_1\tilde{y}_1\frac{x_1v_1\tilde{y}_1}{\tilde{x}_1\tilde{v}_1y_1} + 2a_1\tilde{y}_1 - a_2\tilde{y}_2\frac{x_1v_2\tilde{y}_2}{\tilde{x}_1\tilde{v}_2y_2}\\
&+ 2a_2\tilde{y}_2 + \left(1 - \frac{\tilde{x}_2}{x_2}\right)(d_2\tilde{x}_2 + a_3\tilde{z}_1 + a_4\tilde{z}_2 - d_2x_2) - a_3\tilde{z}_1\frac{x_2v_1\tilde{z}_1}{\tilde{x}_2\tilde{v}_1z_1} + 2a_3\tilde{z}_1\\
&- a_4\tilde{z}_2\frac{x_2v_2\tilde{z}_2}{\tilde{x}_2\tilde{v}_2z_2} + 2a_4\tilde{z}_2 - a_1\tilde{y}_1\frac{y_1\tilde{v}_1}{\tilde{y}_1v_1} - a_3\tilde{z}_1\frac{z_1\tilde{v}_1}{\tilde{z}_1v_1} - a_2\tilde{y}_2\frac{y_2\tilde{v}_2}{\tilde{y}_2v_2} - a_4\tilde{z}_2\frac{z_2\tilde{v}_2}{\tilde{z}_2v_2}\\
=& - d_1\frac{(x_1 - \tilde{x}_1)^2}{x_1} - d_2\frac{(x_2 - \tilde{x}_2)^2}{x_2} + a_1\tilde{y}_1\left(3 - \frac{\tilde{x}_1}{x_1} - \frac{x_1v_1\tilde{y}_1}{\tilde{x}_1\tilde{v}_1y_1} - \frac{y_1\tilde{v}_1}{\tilde{y}_1v_1}\right)\\
&+ a_2\tilde{y}_2\left(3 - \frac{\tilde{x}_1}{x_1} - \frac{x_1v_2\tilde{y}_2}{\tilde{x}_1\tilde{v}_2y_2} - \frac{y_2\tilde{v}_2}{\tilde{y}_2v_2}\right) + a_3\tilde{z}_1\left(3 - \frac{\tilde{x}_2}{x_2} - \frac{x_2v_1\tilde{z}_1}{\tilde{x}_2\tilde{v}_1z_1} - \frac{z_1\tilde{v}_1}{\tilde{z}_1v_1}\right)\\
&+ a_4\tilde{z}_2\left(3 - \frac{\tilde{x}_2}{x_2} - \frac{x_2v_2\tilde{z}_2}{\tilde{x}_2\tilde{v}_2z_2} - \frac{z_2\tilde{v}_2}{\tilde{z}_2v_2}\right).
\end{aligned}$$

Clearly $\frac{d\Theta_2}{dt} \leq 0$ for all $x_1, y_1, y_2, x_2, z_1, z_2, v_1, v_2 > 0$ and $\frac{d\Theta_2}{dt} = 0$ at the steady state SS_3. The solutions of the system tend to $\Xi_2' = \{SS_3\}$. Then L.I.P. implies that SS_3 is G.A.S. □

Under specific biological conditions, both viruses can persist at stable levels simultaneously, regardless of the initial infection levels or disease state. Coexistence occurs when viruses exploit shared or distinct target-cell populations or when immune feedback allows both to survive. This outcome illustrates the potential for multi-virus infections to maintain long-term persistence within a host.

Remark 1. *Examining memory effects in the proposed model through the use of fractional differential equations (FDEs) represents a valuable direction for future research. Fractional-order formulations are well suited to describe systems with nonlocal interactions and hereditary behavior, which frequently arise in biological and epidemiological processes. In recent years, Lyapunov-based methods have been increasingly employed to establish global stability in fractional-order within-host biological models [56–58] as well as in fractional-order epidemiological models [59–61]. In this context, the Lyapunov functions developed in the present study offer a solid analytical basis for extending the model to a fractional-order formulation and for investigating the long-term dynamics of coinfection systems.*

6. Impact of a second target-cell population on two-virus codynamics

This section examines how adding a second target-cell group affects the progression of two viruses. A modified system is considered by including two reverse transcriptase (RT) inhibitors that block fresh

infections. The resulting equations are

$$\begin{cases} \dot{x}_1 = \lambda_1 - d_1 x_1 - (1-\epsilon_1)\beta_1 x_1 v_1 - (1-\epsilon_2)\beta_2 x_1 v_2, \\ \dot{y}_1 = (1-\epsilon_1)\beta_1 x_1 v_1 - a_1 y_1, \\ \dot{y}_2 = (1-\epsilon_2)\beta_2 x_1 v_2 - a_2 y_2, \\ \dot{x}_2 = \lambda_2 - d_2 x_2 - (1-f_1\epsilon_1)\beta_3 x_2 v_1 - (1-f_2\epsilon_2)\beta_4 x_2 v_2, \\ \dot{z}_1 = (1-f_1\epsilon_1)\beta_3 x_2 v_1 - a_3 z_1, \\ \dot{z}_2 = (1-f_2\epsilon_2)\beta_4 x_2 v_2 - a_4 z_2, \\ \dot{v}_1 = k_1 a_1 y_1 + k_3 a_3 z_1 - c_1 v_1, \\ \dot{v}_2 = k_2 a_2 y_2 + k_4 a_4 z_2 - c_2 v_2. \end{cases} \tag{G1}$$

The coefficients $\epsilon_i \in [0,1]$, $i = 1,2$, measure the blocking strength of the two RT inhibitors. Their effect is assumed to be higher in (x_1, y_1, y_2) and reduced in (x_2, z_1, z_2), where the diminished action is written as $f_i\epsilon_i$, with $f_i \in [0,1]$, $i = 1,2$ [62].

The reproduction numbers for system (G1) are given as:

$$\begin{aligned} R_1^{\text{two-target}}(\epsilon_1) &= \frac{(1-\epsilon_1)k_1\beta_1\lambda_1}{c_1 d_1} + \frac{(1-f_1\epsilon_1)k_3\beta_3\lambda_2}{c_1 d_2} = (1-\epsilon_1)R_{11} + (1-f_1\epsilon_1)R_{12}, \\ R_2^{\text{two-target}}(\epsilon_2) &= \frac{(1-\epsilon_2)k_2\beta_2\lambda_1}{c_2 d_1} + \frac{(1-f_2\epsilon_2)k_4\beta_4\lambda_2}{c_2 d_2} = (1-\epsilon_2)R_{21} + (1-f_2\epsilon_2)R_{22}. \end{aligned} \tag{6.1}$$

In the following corollary, we establish the conditions under which at most one virus can persist chronically.

Corollary 1. *For system (G1) and the threshold parameters given in (6.1), the following statements hold:*

- *If $\epsilon_1 \geq \epsilon_{1,\min}^{\text{two-target}}$ and $\epsilon_2 \geq \epsilon_{2,\min}^{\text{two-target}}$, then $R_1^{\text{two-target}}(\epsilon_1) \leq 1$ and $R_2^{\text{two-target}}(\epsilon_2) \leq 1$. In this case, the infection-free steady state, SS_0, is G.A.S.*
- *If $\epsilon_1 < \epsilon_{1,\min}^{\text{two-target}}$ and $\epsilon_2 \geq \epsilon_{2,\min}^{\text{two-target}}$, then $R_1^{\text{two-target}}(\epsilon_1) > 1$ and $R_2^{\text{two-target}}(\epsilon_2) \leq 1$. In this case, the infected v_1-mono-infection steady state, SS_1, is G.A.S.*
- *If $\epsilon_1 \geq \epsilon_{1,\min}^{\text{two-target}}$ and $\epsilon_2 < \epsilon_{2,\min}^{\text{two-target}}$, then $R_1^{\text{two-target}}(\epsilon_1) \leq 1$ and $R_2^{\text{two-target}}(\epsilon_2) > 1$. In this case, the infected v_2-mono-infection steady state, SS_2, is G.A.S.*

We next present the coinfection system with a single target-cell class under the action of two RT inhibitors:

$$\begin{cases} \dot{x}_1 = \lambda_1 - d_1 x_1 - (1-\epsilon_1)\beta_1 x_1 v_1 - (1-\epsilon_2)\beta_2 x_1 v_2, \\ \dot{y}_1 = (1-\epsilon_1)\beta_1 x_1 v_1 - a_1 y_1, \\ \dot{y}_2 = (1-\epsilon_2)\beta_2 x_1 v_2 - a_2 y_2, \\ \dot{v}_1 = k_1 a_1 y_1 - c_1 v_1, \\ \dot{v}_2 = k_2 a_2 y_2 - c_2 v_2, \end{cases} \tag{G2}$$

which has three steady states:

$$\begin{aligned} SS_0^{\text{one-target}} &= \left(x_1^0, 0, 0, 0, 0\right), \\ SS_1^{\text{one-target}} &= \left(\frac{x_1^0}{R_1^{\text{one-target}}(\epsilon_1)}, \frac{c_1 d_1}{(1-\epsilon_1)a_1 k_1 \beta_1}(R_1^{\text{one-target}}(\epsilon_1) - 1), 0, \frac{d_1}{(1-\epsilon_1)\beta_1}(R_1^{\text{one-target}}(\epsilon_1) - 1), 0\right), \end{aligned}$$

$$SS_2^{\text{one-target}} = \left(\frac{x_1^0}{R_2^{\text{one-target}}(\epsilon_2)}, 0, \frac{c_2 d_1}{(1-\epsilon_2) a_2 k_2 \beta_2} (R_2^{\text{one-target}}(\epsilon_2) - 1), 0, \frac{d_1}{(1-\epsilon_2)\beta_2} (R_2^{\text{one-target}}(\epsilon_2) - 1) \right),$$

where

$$R_1^{\text{one-target}}(\epsilon_1) = (1-\epsilon_1) R_{11},$$
$$R_2^{\text{one-target}}(\epsilon_2) = (1-\epsilon_2) R_{21}.$$

It is clear that $R_i^{\text{one-target}}(\epsilon_i) < R_i^{\text{two-target}}(\epsilon_i)$, $i = 1, 2$. Therefore, ignoring the second target-cell population results in an underestimation of the basic reproduction numbers.

The RT inhibitors in systems (G1) and (G2) are designed to block viral entry. We define the minimum drug efficacies $\epsilon_{i,\min}^{\text{one-target}}$ and $\epsilon_{i,\min}^{\text{two-target}}$, $i = 1, 2$, as the smallest values ensuring:

$$R_i^{\text{one-target}}(\epsilon_i) \le 1, \text{ for all } \epsilon_{i,\min}^{\text{one-target}} \le \epsilon_i \le 1,$$
$$R_i^{\text{two-target}}(\epsilon_i) \le 1, \text{ for all } \epsilon_{i,\min}^{\text{two-target}} \le \epsilon_i \le 1, \ i = 1, 2.$$

Let $R_{i1} > 1$, $i = 1, 2$, then

$$\epsilon_{i,\min}^{\text{one-target}} = 1 - \frac{1}{R_{i1}},$$
$$\epsilon_{i,\min}^{\text{two-target}} = \frac{R_{i1} + R_{i2} - 1}{R_{i1} + f_i R_{i2}}, \ i = 1, 2.$$

Since $f_i \in [0, 1]$, $i = 1, 2$, then

$$\epsilon_{i,\min}^{\text{two-target}} = \frac{R_{i1} + R_{i2} - 1}{R_{i1} + f_i R_{i2}} \ge \frac{R_{i1} + R_{i2} - 1}{R_{i1} + R_{i2}} = 1 - \frac{1}{R_{i1} + R_{i2}} > 1 - \frac{1}{R_{i1}} = \epsilon_{i,\min}^{\text{one-target}}, \ i = 1, 2.$$

If the drug level satisfies $\epsilon_{i,\min}^{\text{one-target}} \le \epsilon_i \le \epsilon_{i,\min}^{\text{two-target}}$, then $R_i^{\text{one-target}}(\epsilon_i) \le 1$, which drives system (G2) to the infection-free steady state $SS_0^{\text{One-target}}\left(x_1^0, 0, 0, 0, 0\right)$. However, in the same range, we still have $R_i^{\text{two-target}}(\epsilon_i) > 1$, so the steady state $SS_0^{\text{two-target}}(x_1^0, 0, 0, x_2^0, 0, 0, 0, 0)$ of system (G1) remains unstable. Thus, drug levels determined from the one-target-cell model may not be sufficient to clear the viruses. This highlights the importance of including the second target-cell type in coinfection models to obtain accurate treatment thresholds. Accounting for the extra cell population provides stricter efficacy requirements and a more reliable estimate for successful therapy.

Remark 2. *System (G1) can be formulated as a controlled dynamical system, where $x_1, y_1, y_2, x_2, z_1, z_2, v_1$, and v_2 are the state variables, and ϵ_1 and ϵ_2 represent intervention controls. A variety of control approaches have been employed in epidemiology and virology, including feedback-based methods, adaptive strategies, model predictive control, and optimal control techniques. In particular, optimal treatment policies are commonly formulated by minimizing disease burden while simultaneously accounting for medication costs and adverse side effects. Recent studies in virological modeling, including analyses of HTLV-I dynamics [63] and HIV/HTLV coinfection [24] as well as epidemiological investigations of HIV/AIDS [64] and HIV/TB coinfection [65, 66], demonstrate the effectiveness of optimal control approaches in capturing disease dynamics and evaluating intervention strategies. These contributions highlight the practical value of control-based frameworks and provide strong motivation for extending system (G1) to an optimal control formulation in order to assess and design efficient treatment policies.*

7. Numerical simulations

In this section, the qualitative dynamics of system (2.1)–(2.8) are numerically investigated. The extent to which the simulations confirm the analytical outcomes presented in Theorems 1–4 is assessed using the parameter values in Table 2. The parameter values presented in the table were assumed for the purpose of numerical simulations to illustrate that when the stability conditions are satisfied, all solutions converge to the corresponding equilibrium points. These assumptions are necessary due to the difficulty in estimating the parameters, as real patient data for dual infections are limited. We note that if actual patient data become available, some parameters could be estimated more accurately, allowing for proper validation of the model. System (2.1)–(2.8) is solved using the MATLAB solver ode45. This solver is designed for non-stiff ordinary differential equations and is based on an explicit Runge–Kutta (4,5) scheme. Its adaptive step-size control regulates local errors and provides accurate solutions with moderate computational cost. Owing to its robustness and straightforward implementation within MATLAB, ode45 is well suited for simulating the dynamics of the proposed model.

Table 2. The values of the parameters of model (2.1)–(2.8).

Parameter	Value	Parameter	Value
λ_1	10 cells mm^{-3} day^{-1}	a_2	0.3 day^{-1}
λ_2	5 cells mm^{-3} day^{-1}	a_3	0.1 day^{-1}
d_1	0.01 day^{-1}	a_4	0.2 day^{-1}
d_2	0.01 day^{-1}	k_1	50 virus cells^{-1}
β_1	(Varied) mm^3 virus^{-1} day^{-1}	k_2	40 virus cells^{-1}
β_2	(Varied) mm^3 virus^{-1} day^{-1}	k_3	50 virus cells^{-1}
β_3	(Varied) mm^3 virus^{-1} day^{-1}	k_4	40 virus cells^{-1}
β_4	(Varied) mm^3 virus^{-1} day^{-1}	c_1	3 day^{-1}
a_1	0.5 day^{-1}	c_2	4 day^{-1}

The numerical study is divided into three parts. Subsection 7.1 investigates the stability of all steady states across four regimes (I)–(IV) by varying the four infection rates and examining the asymptotic dynamics of system (2.1)–(2.8) in each regime. Subsection 7.2 examines the impact of RT-inhibitor-based treatment where the reduction in the infection rates is modeled through the parameters for drug efficacy ϵ_i and $f_i\epsilon_i$. Then, it quantifies the stabilization of the resulting viral dynamics. Subsection 7.3 compares our two-target-cell coinfection model with a published HIV-HBV model. This comparison is significant since the incorporation of a second target-cell population necessitates stronger antiviral efficacy thresholds and results in different viral-clearance outcomes compared with the single-target-cell model.

7.1. Stability of the steady states

We begin by investigating the four regimes produced by varying the infection rates $(\beta_1,\beta_2,\beta_3,\beta_4)$ while maintaining all other parameters as the given values in Table 2. We select the following family of initial conditions:

$$\begin{cases} x_1(0) = 600 - 30\ell, & y_1(0) = 2 + 1.5\ell, & y_2(0) = 9 + 0.3\ell, \\ x_2(0) = 400 - 30\ell, & z_1(0) = 10 + 7\ell, & z_2(0) = 0.2 + 3\ell, \\ v_1(0) = 60 + 20\ell, & v_2(0) = 40 + 10\ell, & \ell = 1, 2, ..., 12. \end{cases} \tag{IC1}$$

The threshold parameters R_1, R_2, and the coexistence conditions (C1)–(C3) are those stated in Theorems 1–4. Moreover, we calculate the Jacobian matrix $J = J(x_1, y_1, y_2, x_2, z_1, z_2, v_1, v_2)$ of system (2.1)–(2.8) at each steady state and evaluate the signs of the real parts of its corresponding eigenvalues η_i, $i = 1, 2, ..., 8$, which serves as a numerical check of the local stability results. Consider the Jacobian matrix J given in (5.2). Therefore, we have the following four regimes:

7.1.1. Regime I (spontaneous viral clearance)

With the parameter set $(\beta_1, \beta_2, \beta_3, \beta_4) = (2 \times 10^{-5}, 3 \times 10^{-5}, 3 \times 10^{-5}, 2 \times 10^{-5})$, the threshold value is computed as $R_0 = \max\{R_1, R_2\} = \max\{0.58, 0.40\} \leq 1$. Biologically, this regime represents either strong host immune defenses, low viral infectivity, or effective antiviral intervention, which together prevent either virus from establishing a lasting infection. For all initial conditions listed in (IC1), the trajectories of target cells rise monotonically and approach their limiting values (1000, 500), whereas the infected cells and virus particles of both types decline monotonically and tend to zero (Figure 2). This result reflects full viral clearance and host recovery, indicating that low infection rates are insufficient to sustain long-term viral presence. These simulations support Theorem 1, where system (2.1)–(2.8) always converges to the infection-free steady state $SS_0 = (1000, 0, 0, 500, 0, 0, 0, 0)$. Hence, SS_0 is G.A.S. Consistently, the Jacobian matrix evaluated at SS_0 exhibits eight eigenvalues with strictly negative real parts (Table 3, Regime I), thereby confirming the local asymptotic stability of SS_0.

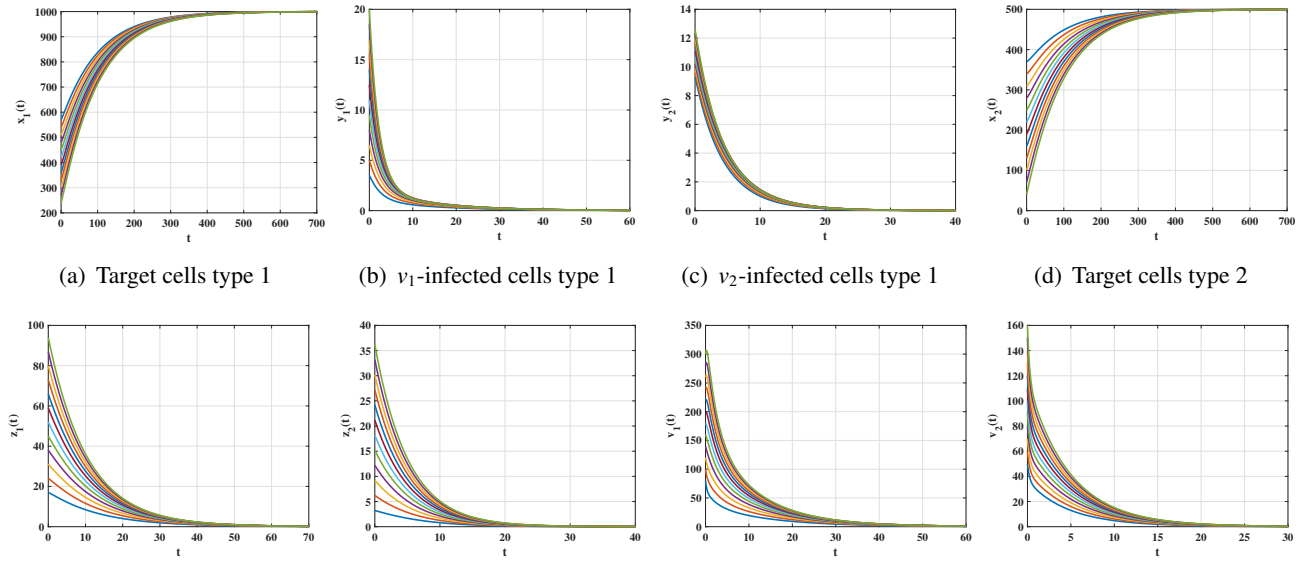

(a) Target cells type 1 (b) v_1-infected cells type 1 (c) v_2-infected cells type 1 (d) Target cells type 2

(e) v_1-infected cells type 2 (f) v_2-infected cells type 2 (g) Virus particles type 1 (h) Virus particles type 2

Figure 2. Dynamics of system (2.1)–(2.8) showing the asymptotic stability of the infection-free steady state $SS_0 = (1000, 0, 0, 500, 0, 0, 0, 0)$ for $R_0 = \max\{R_1, R_2\} \leq 1$ (Regime I).

Table 3. Local stability of nonnegative steady states SS_i, $i = 0, 1, 2, 3$.

Regime	Steady states	(Re(η_i), $i = 1, 2, 3, 4$)	Stability
I	$SS_0 = (1000, 0, 0, 500, 0, 0, 0, 0)$	$(-4.11, -3.21, -0.33, -0.24, -0.15, -0.06, -0.01, -0.01)$	stable
II	$SS_0 = (1000, 0, 0, 500, 0, 0, 0, 0)$	$(-4.44, -4.11, 1.004, -0.24, -0.16, -0.15, -0.01, -0.01)$	unstable
	$SS_1 = (195.46, 16.09, 0, 69.69, 43.03, 0, 205.81, 0)$	$(-4.02, -3.38, -0.28, -0.21, -0.2, -0.04, -0.04, -0.06)$	stable
III	$SS_0 = (1000, 0, 0, 500, 0, 0, 0, 0)$	$(-4.94, -3.21, 0.66, -0.33, -0.22, -0.06, -0.01, -0.01)$	unstable
	$SS_2 = (230.14, 0, 25.66, 154.79, 0, 17.26, 0, 111.51)$	$(-4.27, -3.05, -0.46, -0.23, -0.09, -0.02, -0.02, -0.04)$	stable
IV	$SS_0 = (1000, 0, 0, 500, 0, 0, 0, 0)$	$(-5.34, -4.44, 1.06, 1.004, -0.21, -0.16, -0.01, -0.01)$	unstable
	$SS_1 = (195.46, 16.09, 0, 69.69, 43.03, 0, 205.81, 0)$	$(-4.32, -3.38, -0.21, -0.21, -0.04, -0.04, -0.06, 0.03)$	unstable
	$SS_2 = (141.6, 0, 28.61, 145.99, 0, 17.7, 0, 121.24)$	$(-4.27, -3.32, -0.31, -0.22, -0.03, -0.03, -0.04, 0.03)$	unstable
	$SS_3 = (163.64, 7.31, 15.7, 90.91, 30.44, 5.23, 111.62, 57.58)$	$(-4.28, -3.33, -0.26, -0.22, -0.04, -0.04, -0.03, -0.03)$	stable

7.1.2. Regime II (virus type 1 dominates)

For the parameter values $(\beta_1, \beta_2, \beta_3, \beta_4) = (2 \times 10^{-4}, 3 \times 10^{-5}, 3 \times 10^{-4}, 2 \times 10^{-5})$, the corresponding thresholds are $R_1 = 5.83 > 1$ and $R_2 = 0.40 \leq 1$. Biologically, virus type 1 replicates more efficiently in its preferred target-cell population, allowing it to establish a sustained infection. For all initial conditions listed in (IC1), system (2.1)–(2.8) evolves toward the infected v_1-mono-infection steady state $SS_1 = (195.46, 16.09, 0, 69.69, 43.03, 0, 205.81, 0)$, as predicted by Theorem 2 (Figure 3). As expected in this regime, the infection-free steady state SS_0 is numerically unstable due to one positive eigenvalue, whereas SS_1 is locally asymptotically stable since all eigenvalues corresponding to the Jacobian at SS_1 exhibit negative real parts (Table 3, Regime II). Furthermore, the long-term dynamics across all compartments exhibit the characteristic behavior of a v_1-dominant mono-infection: the populations of target cells tend to positive steady levels, the populations of virus particles and infected cells associated with virus type 1 approach positive steady values, while all virus type 2 associated compartments decline to zero. This pattern illustrates competitive exclusion, in which the more efficient virus inhibits the other strain and prevents its survival. This consistent convergence from all initial conditions corroborates the theoretical outcomes established in Theorem 2 and highlights numerical findings for the global asymptotic stability of the coexistence steady state SS_1.

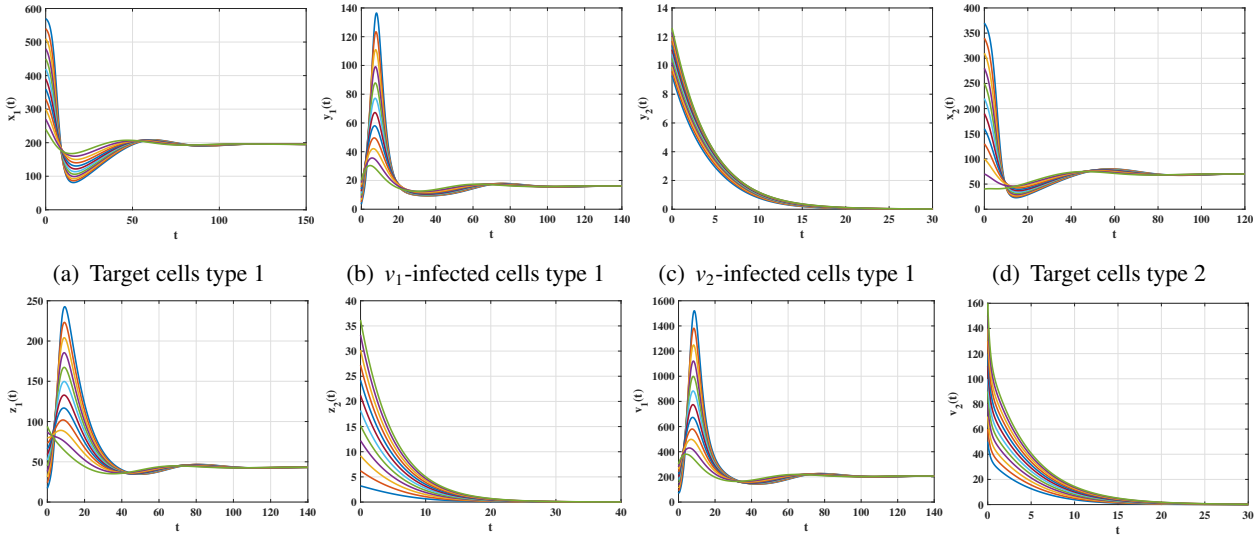

(a) Target cells type 1 (b) v_1-infected cells type 1 (c) v_2-infected cells type 1 (d) Target cells type 2

(e) v_1-infected cells type 2 (f) v_2-infected cells type 2 (g) Virus particles type 1 (h) Virus particles type 2

Figure 3. Dynamics of system (2.1)–(2.8) showing the asymptotic stability of the infected v_1-mono-infection steady state $SS_1 = (195.46, 16.09, 0, 69.69, 43.03, 0, 205.81, 0)$ for $R_1 > 1$ and $R_2 \leq 1$ (Regime II).

7.1.3. Regime III (virus type 2 dominates)

Taking the parameter set $(\beta_1, \beta_2, \beta_3, \beta_4) = (2 \times 10^{-5}, 3 \times 10^{-4}, 3 \times 10^{-5}, 2 \times 10^{-4})$, we obtain $R_2 = 4 > 1$ and $R_1 = 0.58 \leq 1$. In this case, virus type 2 has a higher infection or replication efficiency, which enables it to dominate over virus type 1. Simulations initiated from all initial conditions in (IC1) converge to the infected v_2-mono-infection steady state $SS_2 = (230.14, 0, 25.66, 154.79, 0, 17.26, 0, 111.51)$, in accordance with Theorem 3 (Figure 4). As in the previous regime, SS_0 loses its stability due to one positive eigenvalue, whereas SS_2 is locally asymptotically stable, since the Jacobian at SS_2 possesses eigenvalues with negative real parts (Table 3, Regime III). Compared with Regime II, the long-term dynamics across all compartments exhibit the characteristic behavior of a v_2-dominant mono-infection: The populations of target cells tend to positive steady values, the populations of virus particles and infected cells associated with virus type 2 approach positive steady values, while all virus type 1 associated compartments decline to zero. This regime demonstrates how differences in infection rates influence which virus maintains a long-term presence within the host. This consistent convergence from all initial conditions corroborates the theoretical outcomes established in Theorem 3 and highlights numerical findings for the global asymptotic stability of the coexistence steady state SS_2.

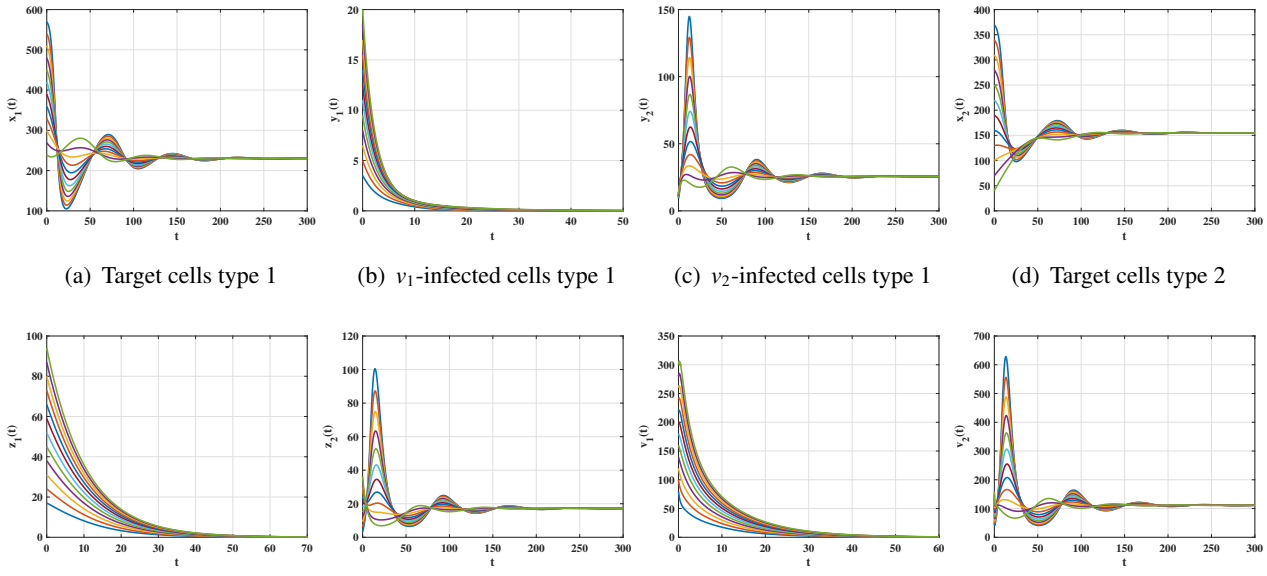

(a) Target cells type 1 (b) v_1-infected cells type 1 (c) v_2-infected cells type 1 (d) Target cells type 2

(e) v_2-infected cells type 2 (f) v_2-infected cells type 2 (g) Virus particles type 1 (h) Virus particles type 2

Figure 4. Dynamics of system (2.1)–(2.8) showing the asymptotic stability of the infected v_2-mono-infection steady state $SS_2 = (230.14, 0, 25.66, 154.79, 0, 17.26, 0, 111.51)$ for $R_2 > 1$ and $R_1 \leq 1$ (Regime III).

7.1.4. Regime IV (coexistence of the two viruses)

Taking the infection rate parameters as $(\beta_1, \beta_2, \beta_3, \beta_4) = (2 \times 10^{-4}, 5 \times 10^{-4}, 3 \times 10^{-4}, 2 \times 10^{-4})$, the coexistence requirements in (C1)–(C3) are fulfilled. The threshold parameters are calculated as

$$R_3 = 3.75 > 1, \qquad \frac{R_{12}}{R_{22}} = 2.5 > 1, \qquad \frac{R_{21}}{R_{11}} = 1.5 > 1,$$

along with the composite inequalities in (C2) and (C3), respectively

$$1.71 > 1 \quad \text{and} \quad 1.45 > 1,$$

ensuring the feasibility of the two-virus coexistence steady state for this parameter regime. Both viruses are able to persist by primarily exploiting distinct target-cell populations, which limits direct competition between them. For all initial conditions specified in (IC1), system (2.1)–(2.8) evolves toward the two-virus coexistence steady state $SS_3 = (163.64, 7.31, 15.7, 90.91, 30.44, 5.23, 111.62, 57.58)$, in accordance with Theorem 4 (Figure 5). As presented in Table 3 (Regime IV), the Jacobian spectra demonstrate that SS_0, SS_1, and SS_2 are unstable in this regime since each of them possesses a positive eigenvalue. In contrast, SS_3 is locally asymptotically stable, as the Jacobian at SS_3 has eigenvalues with negative real parts. The long-term dynamics across all compartments exhibit the characteristic behavior of a coinfection scenario involving two viruses: The populations of target cells settle at positive steady values, the populations of virus particles and infected cells associated with both types stabilize at positive steady values, indicating the persistence of both types of viruses. Such coexistence leads to an effective partitioning of the cellular environment, whereby each virus exhibits maximal replication efficiency in one target cell population and reduced efficiency in the other. As a consequence, both viruses are able to persist simultaneously within the same host.

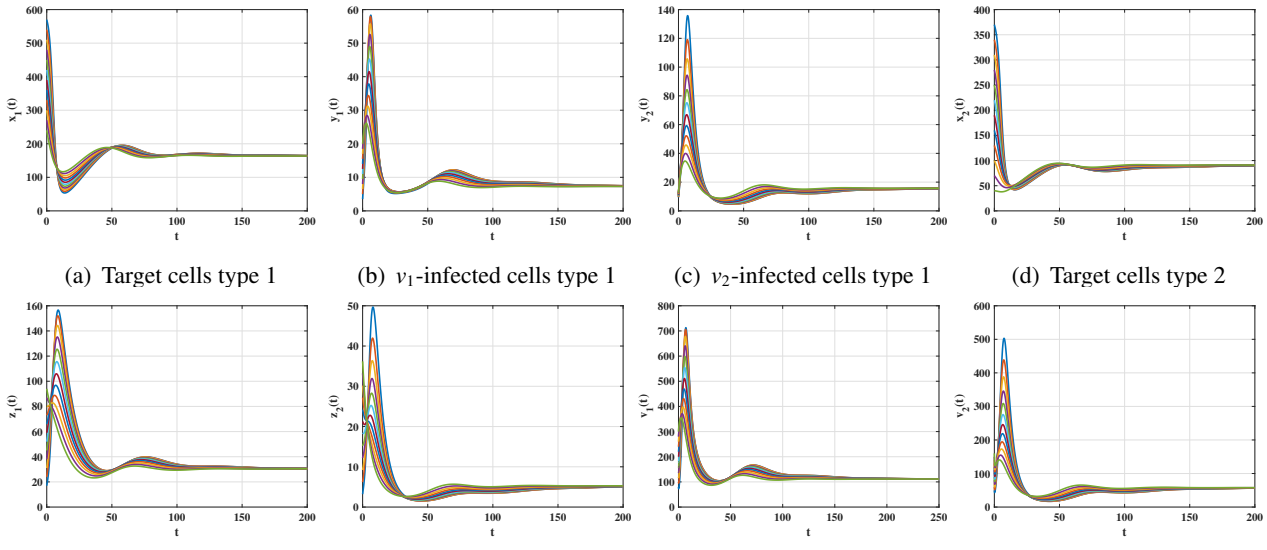

(a) Target cells type 1 (b) v_1-infected cells type 1 (c) v_2-infected cells type 1 (d) Target cells type 2

(e) v_1-infected cells type 2 (f) v_2-infected cells type 2 (g) Virus particles type 1 (h) Virus particles type 2

Figure 5. Dynamics of system (2.1)–(2.8) showing the asymptotic stability of the two-virus coexistence steady state $SS_3 = (163.64, 7.31, 15.7, 90.91, 30.44, 5.23, 111.62, 57.58)$ under conditions C1–C3 (Regime IV).

The preceding analysis shows that changes in the infection rate parameters $(\beta_1, \beta_2, \beta_3, \beta_4)$ can shift the system among four distinct regimes: complete elimination of both viruses, dominance of virus

type 1, dominance of virus type 2, and stable coexistence of the two viral populations. This illustrates how sensitive the within-host dynamics are to viral infectivity and the preference for specific target-cell populations. Likewise, adjusting the drug efficacy parameters ϵ_1 and ϵ_2 reduces the effective infection rates, showing how treatment can shift the system from persistent infection to suppression or complete viral elimination. These findings emphasize the role of parameter variation in capturing realistic disease dynamics and informing treatment strategies.

7.2. Effect of treatments

This subsection discusses the influence of the RT inhibitor-based treatment on the stability properties of system (G1). In order to quantify the lowest therapeutic strength that is essential to control each virus, we use Eq (6.1) to calculate the drug efficacy threshold parameters at $\epsilon_{1,\min}^{\text{two-target}}$ and $\epsilon_{2,\min}^{\text{two-target}}$ so that

$$R_1^{\text{two-target}}(\epsilon_1) = 1 \quad \text{and} \quad R_2^{\text{two-target}}(\epsilon_2) = 1.$$

Then, we take under consideration the parameter values listed in Regime IV and fix $f_1 = f_2 = 0.9$ to obtain the critical $\epsilon_{1,\min}^{\text{two-target}}$ and $\epsilon_{2,\min}^{\text{two-target}}$ as follows:

$$\epsilon_{1,\min}^{\text{two-target}} = \frac{R_{11} + R_{12} - 1}{R_{11} + f_1 R_{12}} = 0.865672,$$
$$\epsilon_{2,\min}^{\text{two-target}} = \frac{R_{21} + R_{22} - 1}{R_{21} + f_2 R_{22}} = 0.847458.$$

To analyze the dynamical behavior of system (G1) under a variety of treatment strengths, we solve system (G1) under the selected initial conditions:

$$\begin{cases} x_1(0) = 600, \quad y_1(0) = 5, \quad y_2(0) = 10, \\ x_2(0) = 300, \quad z_1(0) = 20, \quad z_2(0) = 10, \\ v_1(0) = 60, \quad v_2(0) = 50, \end{cases} \tag{IC2}$$

and examine several selections of (ϵ_1, ϵ_2). The numerical simulations illustrated in Figure 6 and the steady states presented in Table 4 highlight the significant impact of ϵ_1 and ϵ_2 on the dynamics of system (G1). The outcomes are as follows:

- In the absence of treatment ($\epsilon_1 = \epsilon_2 = 0$), both viruses persist and the coinfection becomes chronic. In this situation all solution trajectories converges to SS_3, and it is G.A.S.
- In the moderate treatment level (such as, $\epsilon_1 = \epsilon_2 = 0.75$), both viruses persist and the coinfection becomes chronic. However, a remarkable reduction in the populations of infected cells and virus particles is seen, but still, $R_i^{\text{two-target}} > 1$ for $i = 1, 2$, which guarantees that all solution trajectories converge to SS_3, and it is G.A.S.
- In the case of asymmetric treatment levels ($\epsilon_1 > \epsilon_{1,\min}$ while $\epsilon_2 < \epsilon_{2,\min}$, $\epsilon_1 < \epsilon_{1,\min}$ while $\epsilon_2 > \epsilon_{2,\min}$), particular eradication of one virus is noticed while the other persists, in accordance with virus superiority and $R_i^{\text{two-target}} > 1$ for $i = 1, 2$. In this situation, the solution trajectories converge to the mono-infection state (SS_1 or SS_2).
- In the case that both treatments exceed their minimal values (such as, $\epsilon_1 = \epsilon_2 = 0.9$ or $\epsilon_1 = \epsilon_2$=1), both viruses vanish, and this leads to the healthy situation. Hence, the solution trajectories

converge to the infection-free equilibrium SS_0 where $R_i^{\text{two-target}} \leq 1$ for $i = 1, 2$. These outcomes validate the analytical conditions and confirm that total coinfection clearance demands that both treatment parameters ϵ_1 and ϵ_2 surpass their critical values.

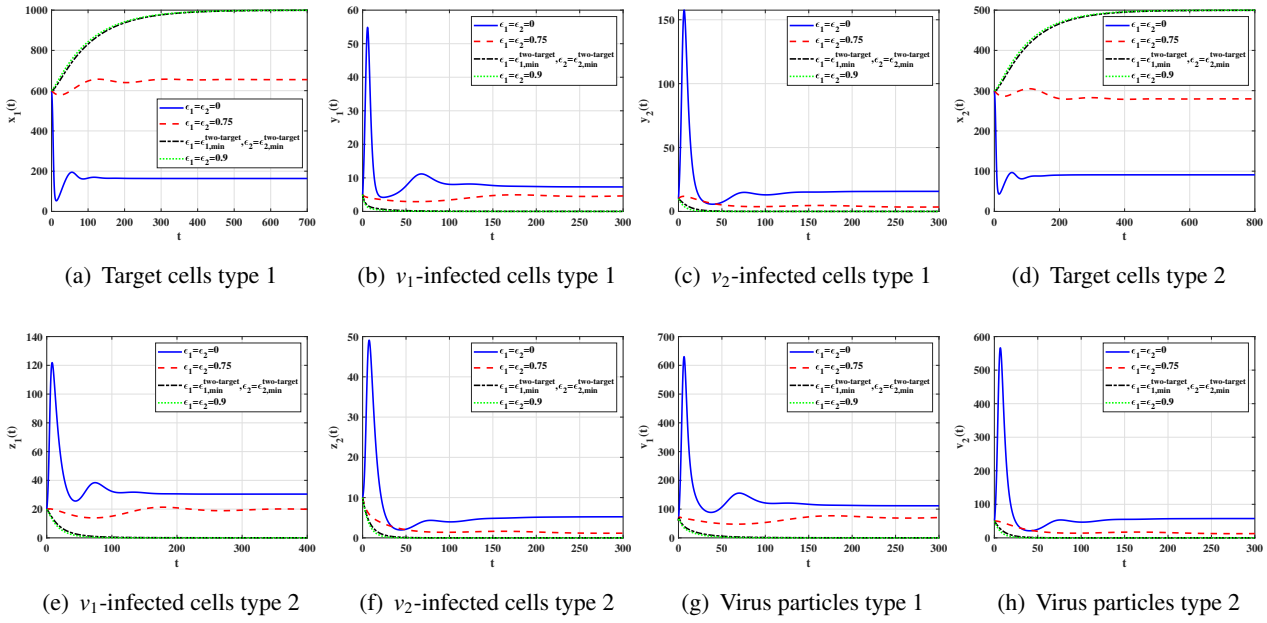

(a) Target cells type 1 (b) v_1-infected cells type 1 (c) v_2-infected cells type 1 (d) Target cells type 2

(e) v_1-infected cells type 2 (f) v_2-infected cells type 2 (g) Virus particles type 1 (h) Virus particles type 2

Figure 6. Dynamics of system (G1) under the effect of RT inhibitor-based treatment.

Table 4. Effect of RT inhibitor-based treatment on the dynamics of system (G1).

Treatment parameters	Steady states	$R_1^{\text{two-target}}(\epsilon_1)$	$R_2^{\text{two-target}}(\epsilon_2)$
$\epsilon_1 = \epsilon_2 = 0$	$SS_3 = (163.64, 7.31, 15.7, 90.91, 30.44, 5.23, 111.62, 57.58)$	5.83	6
$\epsilon_1 = \epsilon_2 = 0.75$	$SS_3 = (654.55, 4.7, 3.69, 279.72, 19.57, 1.23, 71.76, 13.52)$	1.64583	1.575
$\epsilon_1 = 0.9, \epsilon_2 = 0.8$	$SS_2 = (761.74, 0, 7.94, 425.47, 0, 3.73, 0, 31.28)$	0.81	1.28
$\epsilon_1 = 0.8, \epsilon_2 = 0.9$	$SS_1 = (804.61, 3.91, 0, 331.14, 16.89, 0, 60.71, 0)$	1.37	0.69
$\epsilon_1 = 0.865672, \epsilon_2 = 0.847458$	$SS_0 = (1000, 0, 0, 500, 0, 0, 0, 0)$	1	1
$\epsilon_1 = \epsilon_2 = 0.9$	$SS_0 = (1000, 0, 0, 500, 0, 0, 0, 0)$	0.81	0.69
$\epsilon_1 = \epsilon_2 = 1$	$SS_0 = (1000, 0, 0, 500, 0, 0, 0, 0)$	0.25	0.1

7.3. Comparison results

In this subsection, we compare our system (G1) with a previously developed model describing HIV-HBV coinfection given in [27], where both viruses target hepatocytes, while HIV additionally infects $CD4^+$ T cells. The dynamics of HIV and HBV under the influence of two reverse transcriptase inhibitors are formulated as:

$$\begin{cases} \dot{x}_1 = \lambda_1 - d_1 x_1 - (1-\epsilon_1)\beta_1 x_1 v_1 - (1-\epsilon_2)\beta_2 x_1 v_2, \\ \dot{y}_1 = (1-\epsilon_1)\beta_1 x_1 v_1 - a_1 y_1, \\ \dot{y}_2 = (1-\epsilon_2)\beta_2 x_1 v_2 - a_2 y_2, \\ \dot{x}_2 = \lambda_2 - d_2 x_2 - (1-f_1\epsilon_1)\beta_3 x_2 v_1, \\ \dot{z}_1 = (1-f_1\epsilon_1)\beta_3 x_2 v_1 - a_3 z_1, \\ \dot{v}_1 = k_1 a_1 y_1 + k_3 a_3 z_1 - c_1 v_1, \\ \dot{v}_2 = k_2 a_2 y_2 - c_2 v_2. \end{cases} \tag{G3}$$

Here, $x_1(t)$, $y_1(t)$, $y_2(t)$, $x_2(t)$, $z_1(t)$, $v_1(t)$, and $v_2(t)$ represent, respectively, the concentrations of uninfected hepatocytes, HIV-infected hepatocytes, HBV-infected hepatocytes, uninfected $CD4^+$ T cells, HIV-infected $CD4^+$ T cells, free HIV particles, and free HBV particles at time t.

The basic reproduction numbers for system (G3) are given by

$$\begin{aligned} R_1^*(\epsilon_1) &= \frac{(1-\epsilon_1)k_1\beta_1\lambda_1}{c_1 d_1} + \frac{(1-f_1\epsilon_1)k_3\beta_3\lambda_2}{c_1 d_2} = (1-\epsilon_1)R_{11} + (1-f_1\epsilon_1)R_{12}, \\ R_2^*(\epsilon_2) &= \frac{(1-\epsilon_2)k_2\beta_2\lambda_1}{c_2 d_1} = (1-\epsilon_2)R_{21}. \end{aligned}$$

We define the minimum drug efficacies and $\epsilon_{1,\min}^*$, and $\epsilon_{2,\min}^*$, as the smallest values ensuring:

$$R_i^*(\epsilon_i) \le 1, \text{ for all } \epsilon_{i,\min}^* \le \epsilon_i \le 1, \ i = 1, 2,$$

where

$$\epsilon_{1,\min}^* = \frac{R_{11} + R_{12} - 1}{R_{11} + f_1 R_{12}}, \qquad \epsilon_{2,\min}^* = \frac{R_{21} - 1}{R_{21}}.$$

Using the values of the parameters given in Regime IV and choosing $f_1 = f_2 = 0.9$, we get

$$\begin{aligned} \epsilon_{1,\min}^{\text{two-target}} &= \frac{R_{11} + R_{12} - 1}{R_{11} + f_1 R_{12}} = 0.865672, \qquad \epsilon_{2,\min}^{\text{two-target}} = \frac{R_{21} + R_{22} - 1}{R_{21} + f_2 R_{22}} = 0.847458, \\ \epsilon_{1,\min}^{*} &= \frac{R_{11} + R_{12} - 1}{R_{11} + f_1 R_{12}} = 0.865672, \qquad \epsilon_{2,\min}^{*} = \frac{R_{21} - 1}{R_{21}} = 0.8. \end{aligned}$$

In Figure 7, we compare the stability characteristics of systems (G1) and (G3). The initial conditions are chosen as follows:

$$\begin{cases} x_1(0) = 920, \quad y_1(0) = 1, \quad y_2(0) = 3, \\ x_2(0) = 470, \quad z_1(0) = 3, \quad z_2(0) = 1, \\ v_1(0) = 10, \quad v_2(0) = 10. \end{cases} \tag{IC3}$$

We set the drug efficacies $\epsilon_1 = 0.87$ and $\epsilon_2 = 0.82$. Under these values, the effective reproduction numbers become

$$R_1^*(\epsilon_1) = 0.98 < 1, \quad R_2^*(\epsilon_2) = 0.9 < 1,$$

which ensures that system (G3) remains stable at its infection-free equilibrium. In contrast, applying the same efficacies to system (G1) yields

$$R_1^{\text{two-target}}(\epsilon_1) = 0.98 < 1, \quad R_2^{\text{two-target}}(\epsilon_2) = 1.16 > 1,$$

indicating instability of the infection-free state. Therefore, estimating drug thresholds from a simplified model that ignores the secondary target-cell can lead to insufficient therapy and persistence of at least one viral infection. This comparison underscores the necessity of incorporating all relevant target cell populations in coinfection models to derive accurate efficacy thresholds. Including the additional cell type results in stricter, but more realistic, treatment conditions for viral eradication.

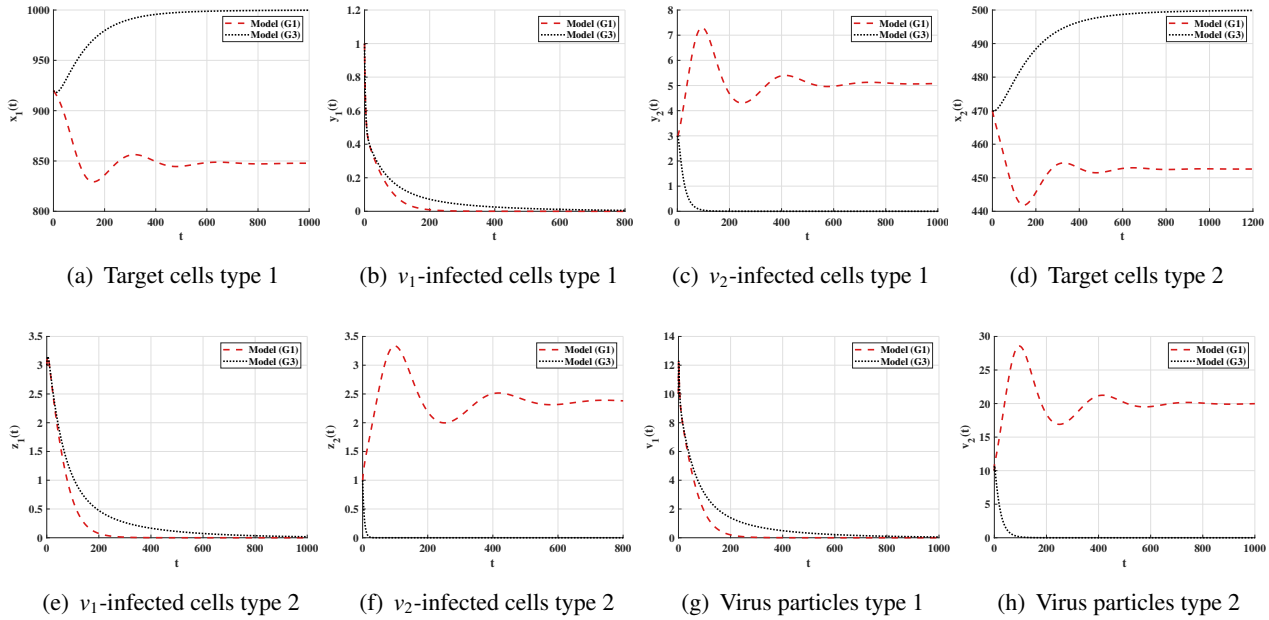

(a) Target cells type 1 (b) v_1-infected cells type 1 (c) v_2-infected cells type 1 (d) Target cells type 2

(e) v_1-infected cells type 2 (f) v_2-infected cells type 2 (g) Virus particles type 1 (h) Virus particles type 2

Figure 7. Solution trajectories for the full two-target infection model (G1) compared with its restricted one-target setting (G3).

Neglecting the second target-cell population can lead to an underestimation of the basic reproduction numbers, which may, in turn, influence clinical decision-making and intervention strategies. To quantify this effect, we evaluate the discrepancy between the two effective reproduction numbers for virus type 2, namely

$$R_2^{\text{two-target}} - R_2^*(\epsilon_2) = 1.16 - 0.9 = 0.26,$$

which corresponds to an approximate difference of 29%. Consequently, treatment strategies developed from models that overlook the second target-cell population of virus type 2 may fail to achieve complete clearance of this virus from the host. Consequently, the treatment efficacy required to eliminate hepatitis C virus type 2 is underestimated by $0.847458-0.82 = 0.027$, corresponding to an approximate discrepancy of 3.35%. This emphasizes the importance of using a mathematical model that accounts for both target-cell types of the two viruses when designing treatment schedules.

7.4. Sensitivity analysis

To assess the influence of each parameter of system (G1) on the threshold quantities defined in (6.1), the normalized forward sensitivity index is employed, as given below:

$$\Lambda_\alpha = \frac{\alpha}{R_i^{\text{two-target}}(\epsilon_i)} \frac{\partial R_i^{\text{two-target}}(\epsilon_i)}{\partial \alpha}, \quad i = 1, 2, \tag{7.1}$$

where α accounts for any parameter of interest. When Λ_α takes a positive value, an increase in α enhances $R_i^{\text{two-target}}(\epsilon_i)$; conversely, a negative value reflects a suppressive impact. Thus, the proportional impact of parameter α on the threshold quantity is quantified by its magnitude of Λ_α. We take into consideration the parameter set used in Regime IV and fix $f_1 = f_2 = 0.9$ and $\epsilon_1 = \epsilon_2 = 0.6$. Then, we use Eq (7.1) to compute the normalized sensitivity indices Λ_α for all parameters associated with Eq (6.1). Tables 5 and 6 summarize all calculated outcomes describing, respectively, the sensitivity of $R_1^{\text{two-target}}(\epsilon_1)$ and $R_2^{\text{two-target}}(\epsilon_2)$ under the chosen parameter values. Figures 8 and 9 present their corresponding graphical representations.

In the subsequent discussion, we outline the main sensitivity outcomes and highlight the parameters that have the greatest effect on the infection dynamics.

Table 5. Sensitivity indices of $R_1^{\text{two-target}}(\epsilon_1)$ associated with the parameters of system (G1).

Parameter α	Λ_α	Parameter α	Λ_α	Parameter α	Λ_α
λ_1	0.537	β_1	0.537	c_1	−1
λ_2	0.463	β_3	0.463	ϵ_1	−1.349
d_1	−0.537	k_1	0.537	f_1	−0.544
d_2	−0.463	k_3	0.463		

Table 6. Sensitivity indices of $R_2^{\text{two-target}}(\epsilon_2)$ associated with the parameters of system (G1).

Parameter α	Λ_α	Parameter α	Λ_α	Parameter α	Λ_α
λ_1	0.813	β_2	0.813	c_2	−1
λ_2	0.187	β_4	0.187	ϵ_2	−1.439
d_1	−0.813	k_2	0.813	f_2	−0.22
d_2	−0.187	k_4	0.187		

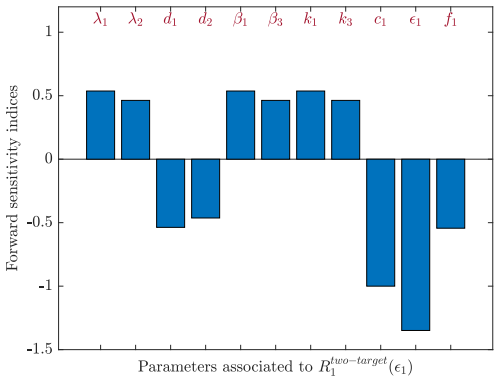

Figure 8. Parameter contribution pattern corresponding to $R_1^{\text{two-target}}(\epsilon_1)$ in system (G1).

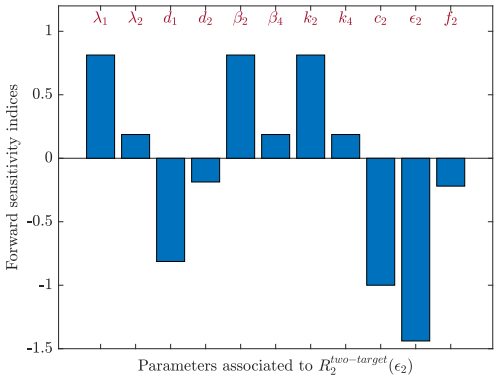

Figure 9. Parameter contribution pattern corresponding to $R_2^{\text{two-target}}(\epsilon_2)$ in system (G1).

7.4.1. Sensitivity of $R_1^{\text{two-target}}(\epsilon_1)$

As reported in Table 5 and displayed in Figure 8, $R_1^{\text{two-target}}(\epsilon_1)$ responds most strongly to the parameters λ_1, β_1, k_1, and ϵ_1. Positive sensitivity indices for λ_1, β_1, and k_1 suggest that enhancing their values increases $R_1^{\text{two-target}}(\epsilon_1)$, thereby supporting the persistence of virus type 1. On the other hand, the RT inhibitor efficacy ϵ_1 attains the highest negative sensitivity index. This strong negative effect is caused by the multiplicative term $(1 - \epsilon_1)$ that appears in the infection rate of system (G1), signifying that even a slight increase in ϵ_1 notably reduces viral replication. Consequently, increasing treatment efficacy plays a crucial role in controlling virus type 1.

7.4.2. Sensitivity of $R_2^{\text{two-target}}(\epsilon_2)$

A similar observation is found for $R_2^{\text{two-target}}(\epsilon_2)$, as reported in Table 6 and illustrated in Figure 9. Positive sensitivity indices for λ_1, β_2, and k_2 suggest that enhancing their values increases $R_2^{\text{two-target}}(\epsilon_2)$, thereby supporting the persistence of virus type 2. However, the RT inhibitor efficacy ϵ_2 attains the highest negative sensitivity index. This strong negative effect is caused by the multiplicative term $(1 - \epsilon_2)$ that appears in the infection rate of system (G1), signifying that even a slight increase in ϵ_2 notably reduces viral replication. Consequently, increasing treatment efficacy plays a crucial role in controlling virus type 2. This sheds light on the importance of including a sufficiently strong inhibitory response in the second target-cell compartment, thereby suppressing viral coexistence and controlling the infection.

8. Conclusions

Earlier models of two-virus coinfection often indicated that chronic infection can occur, but usually for only one virus; stable coexistence of two viruses was rarely predicted. These models commonly include an infection-free steady state, where both viruses are cleared, and two boundary steady states, where either virus type 1 suppresses virus type 2 or vice versa. In other approaches, both viruses share the same target cells, and one of them can also infect another target-cell type. In such cases, a coexistence steady state may arise, allowing both viruses to persist together. Stable coexistence may also appear in models that include superinfection, immune control, or saturation effects. These results

show that the persistence of both viruses depends on the interactions between their target cells and the host's internal regulation.

Based on evidence that many viruses can infect several cell types, we developed and analyzed a two-virus coinfection model in which the viruses infect and compete within two distinct target-cell populations. The model shows that both viruses can coexist and persist, giving a possible explanation for chronic coinfection and the factors that allow such coexistence.

The basic reproduction numbers were obtained for virus type 1 (R_1), virus type 2 (R_2), and the two-virus case ($R_0 = \max\{R_1, R_2\}$). The existence of infection-free, single-infection, and coexistence equilibria was determined, and their stability was established by Lyapunov functions. Biologically, the steady states can be interpreted as follows:

- SS_0 **(Regime I, viral clearance):** Both viruses are cleared ($R_0 \leq 1$), and target cells recover, reflecting low viral infectivity or effective intervention.
- SS_1 **(Regime II, virus type 1 dominance):** Virus type 1 persists ($R_1 > 1$ and $R_2 \leq 1$) while virus type 2 is cleared. This reflects competitive exclusion, where the more efficient virus suppresses the other strain, preventing its survival.
- SS_2 **(Regime III, virus type 2 dominance):** Virus type 2 persists ($R_2 > 1$ and $R_1 \leq 1$) while virus type 1 is cleared, illustrating competitive exclusion.
- SS_3 **(Regime IV, coexistence):** Both viruses persist (Conditions (C1)–(C3) hold) by exploiting distinct target cells, reflecting niche partitioning and long-term coexistence.

Each of the four steady states of the system has been shown to be globally asymptotically stable within its corresponding set of conditions.

We further investigated the impact of including the second target-cell population for both viruses on the system's dynamic behavior. The results show that the second target is necessary for coexistence and increases the reproduction numbers:

$$R_1 = R_{11} + R_{12} > R_{11}, \quad R_2 = R_{21} + R_{22} > R_{21}.$$

Consequently, neglecting the second target-cell population results in underestimated values of R_1 and R_2, potentially compromising the design of treatments capable of fully clearing the viruses from the host.

We examined the impact of antiviral therapy on viral dynamics and observed a marked reduction in viral load. Additionally, we identified the minimum drug efficacy required to satisfy both $R_1 \leq 1$ and $R_2 \leq 1$, thereby stabilizing the uninfected equilibrium and ensuring the elimination of both viruses from the host. To validate these theoretical results, numerical simulations were conducted, highlighting the influence of collision rate parameters β_i, $i = 1, 2, 3, 4$ in producing four distinct outcomes: complete viral clearance, elimination of type 2 virus with persistence of type 1, elimination of type 1 virus with persistence of type 2, and stable coinfection of both viruses. We also compared the proposed model with one that ignores the second target cell for type 2 virus and found that relying on the simplified model may lead to insufficient treatment thresholds. In contrast, our model offers a more accurate and reliable framework for determining the drug efficacy necessary to achieve the successful eradication of both viral types. The enhanced model provides insights into the dynamics of coinfection involving multiple viruses and offers a reliable framework for estimating the therapeutic doses required to achieve complete viral clearance.

One major limitation of this study is the difficulty in accurately estimating the model parameters due to the limited availability of clinical data from patients experiencing dual viral infections. Although data for single-virus infections are more readily obtainable, gathering reliable information for co-infected patients continues to be a considerable challenge.

Based on the findings of this study, the following extensions are suggested: (i) reformulating the model using fractional-order differential equations to capture memory effects in viral codynamics, (ii) integrating real-world clinical data to refine parameter estimates and enhance predictive accuracy, (iii) incorporating the host immune response into the model, and (iv) developing optimal treatment strategies through optimal control theory. These directions offer promising avenues for future research and may increase the model's clinical relevance.

Author contributions

N. H. AlShamrani and A. M. Elaiw: Conceptualization, Methodology, Software, Writing-original draft; Validation; Writing-review and editing. All authors have read and approved the final version of the manuscript for publication.

Use of Generative-AI tools declaration

The authors declare they have not used Artificial Intelligence (AI) tools in the creation of this article.

Acknowledgments

This work was funded by the University of Jeddah, Jeddah, Saudi Arabia, under grant No. (UJ-24-DR-2617-1). Therefore, the authors thank the University of Jeddah for its technical and financial support.

Conflict of interest

The authors declare no conflict of interest.

References

1. R. J. Rockett, J. Draper, M. Gall, E. M. Sim, A. Arnott, J. E. Agius, et al., Co-infection with SARS-CoV-2 Omicron and Delta variants revealed by genomic surveillance, *Nat. Commun.*, **13** (2022), 2745. https://doi.org/10.1038/s41467-022-30518-x
2. S. Bonhoeffer, R. M. May, G. M. Shaw, M. A. Nowak, Virus dynamics and drug therapy, *PNAS*, **94** (1997), 6971–6976. https://doi.org/10.1073/pnas.94.13.6971
3. S. B. Halstead, Pathogenesis of dengue: challenges to molecular biology, *Science*, **239** (1988), 476–481. https://doi.org/10.1126/science.3277268
4. E. Pilotti, M. V. Bianchi, A. De Maria, F. Bozzano, M. G. Romanelli, U. Bertazzoni, et al., HTLV-1/-2 and HIV-1 co-infections: retroviral interference on host immune status, *Front. Microbiol.*, **4** (2013), 372. https://doi.org/10.3389/fmicb.2013.00372

5. Q. Maqsood, A. Sumrin, M. Iqbal, S. Younas, N. Hussain, M. Mahnoor, et al., Hepatitis C virus/Hepatitis B virus coinfection: current prospectives, *Antivir. Ther.*, **28** (2023), 1–18. https://doi.org/10.1177/13596535231189643

6. E. Zappulo, A. Giaccone, N. Schiano Moriello, I. Gentile, Pharmacological approaches to prevent vertical transmission of HIV and HBV, *Expert Rev. Clin. Phar.*, **15** (2022), 863–876. https://doi.org/10.1080/17512433.2022.2105202

7. A. Omame, M. E. Isah, M. Abbas, An optimal control model for COVID-19, zika, dengue, and chikungunya co-dynamics with reinfection, *Optim. Contr. Appl. Meth.*, **44** (2023), 170–204. https://doi.org/10.1002/oca.2936

8. K. Murphy, SARS CoV-2 detection from upper and lower respiratory tract specimens: diagnostic and infection control implications, *Chest*, **158** (2020), 1804–1805. https://doi.org/10.1016/j.chest.2020.07.061

9. M. A. Nowak, C. R. M. Bangham, Population dynamics of immune responses to persistent viruses, *Science*, **272** (1996), 74–79. https://doi.org/10.1126/science.272.5258.74

10. X. Lai, X. Zou, Modeling HIV-1 virus dynamics with both virus-to-cell infection and cell-to-cell transmission, *SIAM J. Appl. Math.*, **74** (2014), 898–917. https://doi.org/10.1137/130930145

11. Y. Yang, L. Zou, S. Ruan, Global dynamics of a delayed within-host viral infection model with both virus-to-cell and cell-to-cell transmissions, *Math. Biosci.*, **270** (2015), 183–191. https://doi.org/10.1016/j.mbs.2015.05.001

12. D. Hu, Y. Yuan, Threshold dynamics of an age-structured HIV model with virus-to-cell, cell-to-cell transmissions, and CTL immune response, *J. Math. Biol.*, **92** (2026), 13. https://doi.org/10.1007/s00285-025-02328-4

13. G. Doitsh, N. Galloway, X. Geng, Z. Yang, K. Monroe, O. Zepeda, et al., Cell death by pyroptosis drives CD4 T-cell depletion in HIV-1 infection, *Nature*, **505** (2014), 509–514. https://doi.org/10.1038/nature12940

14. Y. Jiang, T. Zhang, Global stability of a cytokine-enhanced viral infection model with nonlinear incidence rate and time delays, *Appl. Math. Lett.*, **132** (2022), 108110. https://doi.org/10.1016/j.aml.2022.108110

15. W. Wang, G. Wu, X. Fan, Global dynamics of a novel viral infection model mediated by pattern recognition receptors, *Appl. Math. Lett.*, **173** (2026), 109757. https://doi.org/10.1016/j.aml.2025.109757

16. P. A. Naik, B. M. Yeolekar, S. Qureshi, N. Manhas, M. Ghoreishi, M. Yeolekar et al., Global analysis of a fractional-order hepatitis B virus model under immune response in the presence of cytokines, *Adv. Theor. Simul.*, **7** (2024), 2400726. https://doi.org/10.1002/adts.202400726

17. W. Wang, X. Wang, X. Fan, On the global attractivity of a diffusive viral infection model with spatial heterogeneity, *Math. Method. Appl. Sci.*, **48** (2025), 15656–15660. https://doi.org/10.1002/mma.70040

18. G. Huang, Y. Takeuchi, W. Ma, Lyapunov functionals for delay differential equations model of viral infections, *SIAM J. Appl. Math.*, **70** (2010), 2693–2708. https://doi.org/10.1137/090780821

19. L. Hong, J. Li, L. Rong, X. Wang, Global dynamics of a delayed model with cytokine-enhanced viral infection and cell-to-cell transmission, *AIMS Mathematics*, **9** (2024), 16280–16296. https://doi.org/10.3934/math.2024788

20. P. De Leenheer, S. S. Pilyugin, Multistrain virus dynamics with mutations: a global analysis, *Math. Med. Biol.*, **25** (2008), 285–322. https://doi.org/10.1093/imammb/dqn023

21. L. Pinky, H. M. Dobrovolny, SARS-CoV-2 coinfections: could influenza and the common cold be beneficial? *J. Med. Virol.*, **92** (2020), 2623–2630. https://doi.org/10.1002/jmv.26098

22. L. Pinky, G. Gonzalez-Parra, H. M. Dobrovolny, Superinfection and cell regeneration can lead to chronic viral coinfections, *J. Theor. Biol.*, **466** (2019), 24–38. https://doi.org/10.1016/j.jtbi.2019.01.011

23. A. M. Elaiw, N. H. AlShamrani, Analysis of a within-host HIV/HTLV-I co-infection model with immunity, *Virus Res.*, **295** (2021), 198204. https://doi.org/10.1016/j.virusres.2020.198204

24. R. Shi, Y. Zhang, Dynamic analysis and optimal control of a fractional order HIV/HTLV co-infection model with HIV-specific CTL immune response, *AIMS Mathematics*, **9** (2024), 9455–9493. https://doi.org/10.3934/math.2024462

25. A. M. Elaiw, A. D. Al Agha, G. Alsaadi, A. D. Hobiny, Global analysis of HCV/HBV codynamics model with antibody immunity, *Eur. Phys. J. Plus*, **139** (2024), 850. https://doi.org/10.1140/epjp/s13360-024-05604-2

26. A. M. Elaiw, G. Alsaadi, A. A. Raezah, A. D. Hobiny, Co-dynamics of hepatitis B and C viruses under the influence of CTL immunity, *Alex. Eng. J.*, **119** (2025), 285–325. https://doi.org/10.1016/j.aej.2025.01.029

27. H. Nampala, L. S. Luboobi, J. Y. Mugisha, C. Obua, M. Jablonska-Sabuka, Modelling hepatotoxicity and antiretroviral therapeutic effect in HIV/HBV co-infection, *Math. Biosci.*, **302** (2018), 67–79. https://doi.org/10.1016/j.mbs.2018.05.012

28. R. Shi, T. Lu, C. Wang, Dynamic analysis of a fractional-order model for HIV with drug-resistance and CTL immune response, *Math. Comput. Simulat.*, **188** (2021), 509–536. https://doi.org/10.1016/j.matcom.2021.04.022

29. A. M. Elaiw, R. S. Alsulami, A. D. Hobiny, Global properties of SARS-CoV-2 and IAV coinfection model with distributed-time delays and humoral immunity, *Math. Method. Appl. Sci.*, **47** (2024), 9340–9384. https://doi.org/10.1002/mma.10074

30. M. S. Khumaeroh, N. Nuwari, E. S. Erianto, N. Rizka, Mathematical model of SAR-CoV-2 and influenza a virus coinfection within host with CTL-mediated immunity, *JJBM*, **5** (2024), 95–108. https://doi.org/10.37905/jjbm.v5i2.27782

31. A. M. Elaiw, N. H. AlShamrani, A. D. Hobiny, Mathematical modeling of HIV/HTLV co-infection with CTL-mediated immunity, *AIMS Mathematics*, **6** (2020), 1634–1676. https://doi.org/10.3934/math.2021098

32. H. Yang, X. Li, W. Zhang, A stochastic HIV/HTLV-I co-infection model incorporating the AIDS-related cancer cells, *Discrete Cont. Dyn.-B*, **29** (2024), 702–730. https://doi.org/10.3934/dcdsb.2023110

33. S. Chowdhury, J. K. Ghosh, U. Ghosh, Co-infection dynamics between HIV-HTLV-I disease with the effects of cytotoxic T-lymphocytes, saturated incidence rate and study of optimal control, *Math. Comput. Simulat.*, **223** (2024), 195–218. https://doi.org/10.1016/j.matcom.2024.04.015

34. A. Nurtay, M. G. Hennessy, J. Sardanyés, L. Alsedà, S. F. Elena, Theoretical conditions for the coexistence of viral strains with differences in phenotypic traits: a bifurcation analysis, *R. Soc. Open Sci.*, **6** (2019), 181179. https://doi.org/10.1098/rsos.181179

35. Y. He, W. Ma, S. Dang, L. Chen, R. Zhang, S. Mei, et al., Possible recombination between two variants of concern in a COVID-19 patient, *Emerg. Microbes Infec.*, **11** (2022), 552–555. https://doi.org/10.1080/22221751.2022.2032375

36. L. B. Rong, R. Ribeiro, A. Perelson, Modeling quasispecies and drug resistance in hepatitis C patients treated with a protease inhibitor, *Bull. Math. Biol.*, **74** (2012), 1789–1817. https://doi.org/10.1007/s11538-012-9736-y

37. L. Rong, Z. Feng, A. S. Perelson, Emergence of HIV-1 drug resistance during antiretroviral treatment, *Bull. Math. Biol.*, **69** (2007), 2027–2060. https://doi.org/10.1007/s11538-007-9203-3

38. P. Wu, H. Zhao, Dynamics of an HIV infection model with two infection routes and evolutionary competition between two viral strains, *Appl. Math. Model.*, **84** (2020), 240–264. https://doi.org/10.1016/j.apm.2020.03.040

39. W. Chen, L. Zhang, N. Wang, Z. Teng, Bifurcation analysis and chaos for a double-strains HIV coinfection model with intracellular delays, saturated incidence and logistic growth, *Math. Comput. Simulat.*, **223** (2024), 617–641. https://doi.org/10.1016/j.matcom.2024.04.025

40. D. Wodarz, *Killer cell dynamics: mathematical and computational approaches to immunology*, New York: Springer, 2007. https://doi.org/10.1007/978-0-387-68733-9

41. S. K. Masenga, B. C. Mweene, E. Luwaya, L. Muchaili, M. Chona, A. Kirabo, HIV-host cell interactions, *Cells*, **12** (2023), 1351. https://doi.org/10.3390/cells12101351

42. C. Gross, A. K. Thoma-Kress, Molecular mechanisms of HTLV-1 cell-to-cell transmission, *Viruses*, **8** (2016), 74. https://doi.org/10.3390/v8030074

43. S. K. Sasmal, Y. Takeuchi, S. Nakaoka, T-cell mediated adaptive immunity and antibody-dependent enhancement in secondary dengue infection, *J. Theor. Biol.*, **470** (2019), 50–63. https://doi.org/10.1016/j.jtbi.2019.03.010

44. S. Jindadamrongwech, C. Thepparit, D. R. Smith, Identification of GRP78 (BiP) as a liver cell-expressed receptor element for dengue virus serotype 2, *Arch. Virol.*, **149** (2004), 915–927. https://doi.org/10.1007/s00705-003-0263-x

45. J. M. Willey, L. M. Sherwood, C. J. Woolverton, *Microbiology*, New York: McGraw-Hill, 2008.

46. F. M. Lum, L. F. P. Ng, Cellular and molecular mechanisms of chikungunya pathogenesis, *Antivir. Res.*, **120** (2015), 165–174. https://doi.org/10.1016/j.antiviral.2015.06.009

47. Z. Her, B. Malleret, M. Chan, E. K. Ong, S. C. Wong, D. J. Kwek, et al., Active infection of human blood monocytes by Chikungunya virus triggers an innate immune response, *J. Immunol.*, **184** (2010), 5903–5913. https://doi.org/10.4049/jimmunol.0904181

48. J. Eder, E. Zijlstra-Willems, G. Koen, N. A. Kootstra, K. C. Wolthers, T. B. Geijtenbeek, Transmission of Zika virus by dendritic cell subsets in skin and vaginal mucosa, *Front. Immunol.*, **14** (2023), 1125565. https://doi.org/10.3389/fimmu.2023.1125565

49. R. Qesmi, J. Wu, J. Wu, J. M. Heffernan, Influence of backward bifurcation in a model of hepatitis B and C viruses, *Math. Biosci.*, **224** (2010), 118–125. https://doi.org/10.1016/j.mbs.2010.01.002

50. R. Qesmi, S. ElSaadany, J. M. Heffernan, J. Wu, A hepatitis B and C virus model with age since infection that exhibits backward bifurcation, *SIAM J. Appl. Math.*, **71** (2011), 1509–1530. https://doi.org/10.1137/10079690X

51. B. Song, Y. Zhang, Y. Sang, L. Zhang, Stability and Hopf bifurcation on an immunity delayed HBV/HCV model with intra- and extra-hepatic coinfection and saturation incidence, *Nonlinear Dyn.*, **111** (2023), 14485–14511. https://doi.org/10.1007/s11071-023-08580-x

52. H. L. Smith, P. Waltman, *The theory of the chemostat: dynamics of microbial competition*, Cambridge: Cambridge University Press, 1995. https://doi.org/10.1017/CBO9780511530043

53. A. Korobeinikov, Global properties of basic virus dynamics models, *Bull. Math. Biol.*, **66** (2004), 879–883. https://doi.org/10.1016/j.bulm.2004.02.001

54. J. K. Hale, S. M. Verduyn Lunel, *Introduction to functional differential equations*, New York: Springer, 1993. https://doi.org/10.1007/978-1-4612-4342-7

55. H. K. Khalil, *Nonlinear systems*, Upper Saddle River: Prentice Hall, 2002.

56. J. Danane, K. Allali, Z. Hammouch, Mathematical analysis of a fractional differential model of HBV infection with antibody immune response, *Chaos Soliton. Fract.*, **136** (2020), 109787. https://doi.org/10.1016/j.chaos.2020.109787

57. Z. Yaagoub, M. Sadki, K. Allali, A generalized fractional hepatitis B virus infection model with both cell-to-cell and virus-to-cell transmissions, *Nonlinear Dyn.*, **112** (2024), 16559–16585. https://doi.org/10.1007/s11071-024-09867-3

58. P. A. Naik, M. Farman, S. Jamil, M. U. Saleem, K. S. Nisar, Z. Huang, Modeling and computational study of cancer treatment with radiotherapy using real data, *PLoS One*, **20** (2025), e0320906. https://doi.org/10.1371/journal.pone.0320906

59. E. F. Obiajulu, N. O. Iheonu, N. N. Araka, A. Omame, Stability and bifurcation analysis in a co-dynamical model for mpox and syphilis incorporating intervention measures using real data from USA, *Model. Earth Syst. Environ.*, **12** (2026), 59. https://doi.org/10.1007/s40808-025-02666-8

60. P. A. Naik, B. M. Yeolekar, S. Qureshi, M. Yeolekar, A. Madzvamuse, Modeling and analysis of the fractional-order epidemic model to investigate mutual influence in HIV/HCV co-infection, *Nonlinear Dyn.*, **112** (2024), 11679–11710. https://doi.org/10.1007/s11071-024-09653-1

61. A. Ahmad, M. Farman, P. A. Naik, E. Hincal, F. Iqbal, Z. Huang, Bifurcation and theoretical analysis of a fractional-order Hepatitis B epidemic model incorporating different chronic stages of infection, *J. Appl. Math. Comput.*, **71** (2025), 1543–1564. https://doi.org/10.1007/s12190-024-02301-2

62. D. S. Callaway, A. S. Perelson, HIV-1 infection and low steady state viral loads, *Bull. Math. Biol.*, **64** (2002), 29–64. https://doi.org/10.1006/bulm.2001.0266

63. S. Khajanchi, S. Bera, T. K. Kar, An optimal control problem for HTLV-I infection model, *Optim. Contr. Appl. Met.*, **46** (2025), 798–810. https://doi.org/10.1002/oca.3232

64. S. W. Teklu, T. T. Guya, B. S. Kotola, T. S. Lachamo, Analyses of an age structure HIV/AIDS compartmental model with optimal control theory, *Sci. Rep.*, **15** (2025), 5491. https://doi.org/10.1038/s41598-024-82467-8

65. L. Yu, S. Gao, X. Z. Li, M. Martcheva, Optimal control of HIV/AIDS-TB co-infection model with health education and treatment, *J. Biol. Syst.*, **33** (2025), 729–779. https://doi.org/10.1142/S0218339025500202

66. A. S. Devi, P. A. Naik, S. Boulaaras, N. Sene, Z. Huang, Understanding the transmission mechanism of HIV/TB co-infection using fractional framework with optimal control, *Int. J. Numer. Model. Electron.*, **38** (2025), e70097. https://doi.org/10.1002/jnm.70097

67. P. van den Driessche, J. Watmough, Reproduction numbers and sub-threshold endemic equilibria for compartmental models of disease transmission, *Math. Biosci.*, **180** (2002), 29–48. https://doi.org/10.1016/S0025-5564(02)00108-6

Appendix. Basic reproduction number

The basic reproduction number represents the expected number of secondary infections generated by a single infected cell during its entire infectious period, assuming that all target cells are initially uninfected. This quantity is evaluated at the infection-free steady state.

A.1. Calculation of the basic reproduction number for a single-virus model

The subsystem corresponding to infection by virus type 1 is obtained by removing all variables associated with virus type 2. This is accomplished by assigning $v_2 = y_2 = z_2 = 0$ in Eqs (2.1)–(2.8), which leads to the following reduced model:

$$\dot{x}_1 = \lambda_1 - d_1 x_1 - \beta_1 x_1 v_1, \tag{A.1}$$

$$\dot{y}_1 = \beta_1 x_1 v_1 - a_1 y_1, \tag{A.2}$$

$$\dot{x}_2 = \lambda_2 - d_2 x_2 - \beta_3 x_2 v_1, \tag{A.3}$$

$$\dot{z}_1 = \beta_3 x_2 v_1 - a_3 z_1, \tag{A.4}$$

$$\dot{v}_1 = k_1 a_1 y_1 + k_3 a_3 z_1 - c_1 v_1. \tag{A.5}$$

The infection-free equilibrium of system (A.1)–(A.5) is

$$SS_0 = (x_1^0, 0, x_2^0, 0, 0).$$

The basic reproduction number R_1 is computed as the dominant eigenvalue of the next-generation matrix $\rho(F_1 V_1^{-1})$. The matrix F_1 contains the new infection terms, and V_1 includes the transition terms between infected classes, constructed using the method of [67]. The matrices are

$$F_1 = \begin{pmatrix} 0 & 0 & \dfrac{\beta_1 \lambda_1}{d_1} \\ 0 & 0 & \dfrac{\beta_3 \lambda_2}{d_2} \\ 0 & 0 & 0 \end{pmatrix}, \qquad V_1 = \begin{pmatrix} a_1 & 0 & 0 \\ 0 & a_3 & 0 \\ -a_1 k_1 & -a_3 k_3 & c_1 \end{pmatrix}.$$

Accordingly, the basic reproduction number corresponding to a v_1-only infection is given by

$$R_1 = \rho(F_1 V_1^{-1}) = R_{11} + R_{12},$$

where

$$R_{11} = \frac{k_1\beta_1\lambda_1}{c_1 d_1}, \qquad R_{12} = \frac{k_3\beta_3\lambda_2}{c_1 d_2}.$$

Here, R_{11} represents the expected number of infections generated by virus type 1 within the x_1 target-cell population, whereas R_{12} captures the contribution of infections occurring in the x_2 cell compartment.

Similarly we define the basic reproduction number corresponding to a v_2-only infection:

$$R_2 = R_{21} + R_{22}, \qquad R_{21} = \frac{k_2\beta_2\lambda_1}{c_2 d_1}, \qquad R_{22} = \frac{k_4\beta_4\lambda_2}{c_2 d_2}.$$

A.2. Deriving the reproduction number for the two-virus coinfection model

We apply the next-generation method to system (2.1)–(2.8). Let F_0 collect the new infection terms and V_0 contain the transition and removal terms. The basic reproduction number is $R_0 = \rho(F_0 V_0^{-1})$. The matrices are

$$F_0 = \begin{pmatrix} 0 & 0 & 0 & 0 & \frac{\beta_1\lambda_1}{d_1} & 0 \\ 0 & 0 & 0 & 0 & 0 & \frac{\beta_2\lambda_1}{d_1} \\ 0 & 0 & 0 & 0 & \frac{\beta_3\lambda_2}{d_2} & 0 \\ 0 & 0 & 0 & 0 & 0 & \frac{\beta_4\lambda_2}{d_2} \\ 0 & 0 & 0 & 0 & 0 & 0 \\ 0 & 0 & 0 & 0 & 0 & 0 \end{pmatrix}, \qquad V_0 = \begin{pmatrix} a_1 & 0 & 0 & 0 & 0 & 0 \\ 0 & a_2 & 0 & 0 & 0 & 0 \\ 0 & 0 & a_3 & 0 & 0 & 0 \\ 0 & 0 & 0 & a_4 & 0 & 0 \\ -a_1k_1 & 0 & -a_3k_3 & 0 & c_1 & 0 \\ 0 & -a_2k_2 & 0 & -a_4k_4 & 0 & c_2 \end{pmatrix}.$$

Thus,

$$R_0 = \rho(F_0 V_0^{-1}) = \max\left\{\frac{k_1\beta_1\lambda_1}{c_1 d_1} + \frac{k_3\beta_3\lambda_2}{c_1 d_2}, \frac{k_2\beta_2\lambda_1}{c_2 d_1} + \frac{k_4\beta_4\lambda_2}{c_2 d_2}\right\} = \max\{R_1, R_2\}.$$

Biological considerations: R_0 measures the expected number of secondary infections produced by a single infected cell in an otherwise uninfected host. Each term reflects contributions from specific target-cell populations. For virus 1, $R_1 = R_{11} + R_{12}$, with R_{11} representing infections in the primary cells x_1 and R_{12} in the secondary cells x_2. Similarly, $R_2 = R_{21} + R_{22}$ for virus 2. A value of $R_0 > 1$ indicates that the infection can establish and spread, while $R_0 \leq 1$ implies that the infection will die out. Breaking R_0 into these components highlights which virus or cell population dominates the dynamics and provides insight into which pathways are critical for viral proliferation, which can guide targeted interventions or therapies.